Attenuating (Sub)Nanometre Vibrations Using Piezoelectric Shunt Damping

A MSc. Thesis

R. R. E. Klöpping

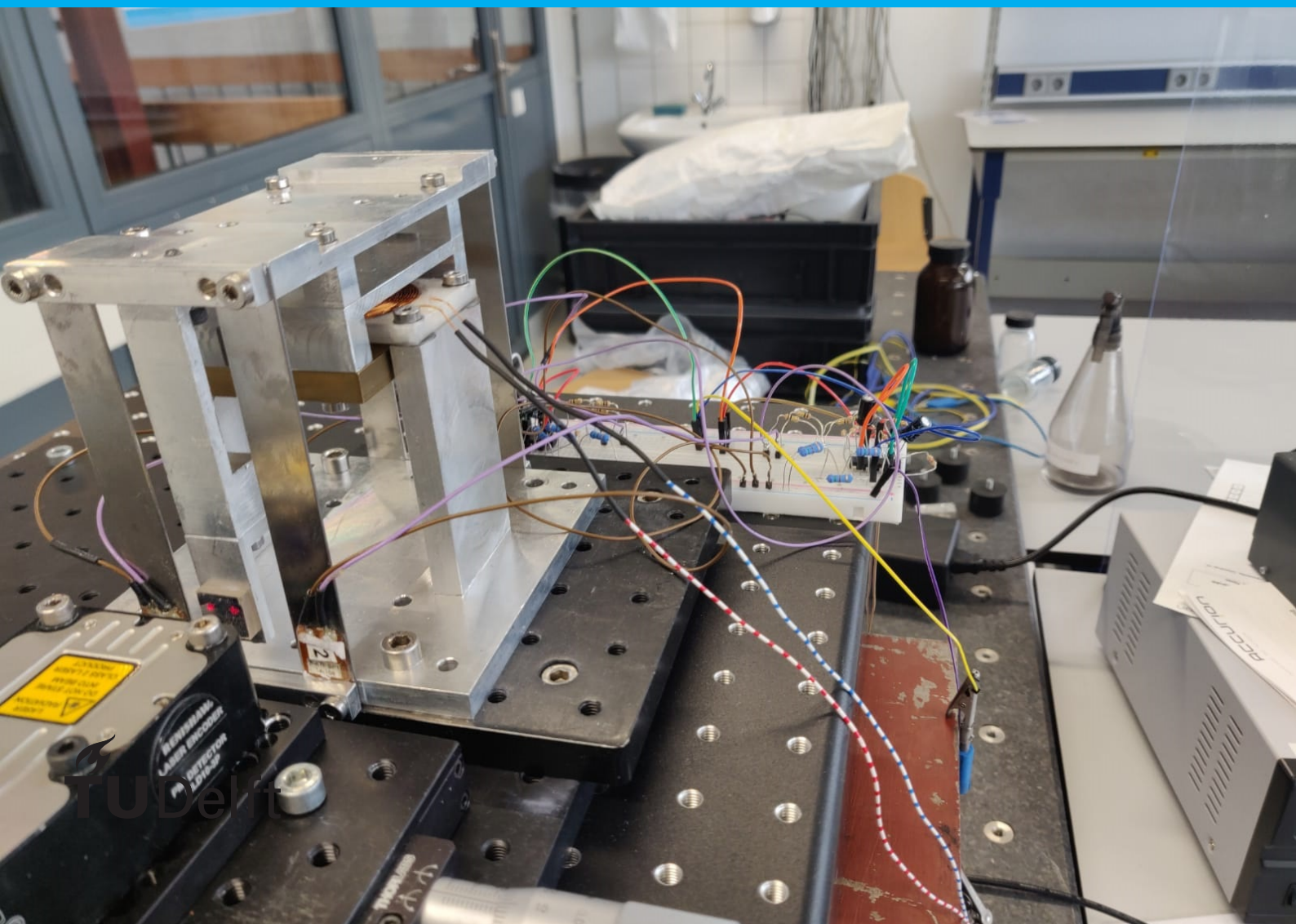

Attenuating (Sub)Nanometre Vibrations Using Piezoelectric Shunt Damping

A MSc. Thesis

by

R. R. E. Klöpping

to obtain the degree of Master of Science
at the Delft University of Technology,
to be defended publicly on Tuesday July 13, 2021 at 09:00 AM.

Student number:	4186508	
Project duration:	April 19, 2020 – July 13, 2021	
Thesis committee:	Dr. S. H. HosseinNia ,	TU Delft, supervisor
	Dr. N. J. Myers,	TU Delft
	D. van Grinsven,	Settels Savenije van Amelsvoort, supervisor
	Ir. E. Hilders,	Settels Savenije van Amelsvoort, supervisor

An electronic version of this thesis is available at `http://repository.tudelft.nl/`.

TU Delft

Abstract

Settels Savenije van Amelsvoort is interested in investigating the use of piezoelectric shunt damping for a measurement and calibrations setup. The goal is to damp the remaining vibrations from previous vibration isolation stages to sub-nanometre amplitude. There was interest in piezoelectric shunt damping as a damping mechanism. Although piezoelectric shunt damping has previously been achieved at nanometre level and high frequency, the use of piezoelectric shunt damping at (sub)nanometre amplitude and low resonance frequency is still an open challenge and a novel application.

In order to test the feasibility of this application, a test setup is constructed. The experiment is performed on several vibrations isolation stages and with two different shunts. The final setup is able to damp the vibrations at 100 nm and indicates that it can damp vibrations at 50 nm. However, the results at 50 nm are inconclusive due to the resolution of the sensor and vibrations induced by the ground motion. For future research it is recommended to increase the vibration isolation and to use a sensor with higher resolution, this might show that damping at sub-nanometre amplitudes is feasible.

Contents

1

Introduction

1.1. Problem Statement

Settels Savenije van Amelsvoort is interested in investigating the use of piezoelectric shunt damping for the purpose of damping the remaining vibrations in a setup upon which measurements and calibrations can be performed. In order for these measurements and calibrations to be done, external vibrations and the ground motion need to be attenuated. This setup consists of multiple vibration isolation stages, which reduce the amplitude of the ground motion to (sub)nanometres. A sketch of this setup with passive vibration isolation only in vertical direction is shown in figure 1.1. As can be seen there are three stages of vibration isolation within the setup. In the last stage, there will remain vibrations of sub-nanometre amplitude and these vibrations need to be damped using piezoelectric shunt damping.

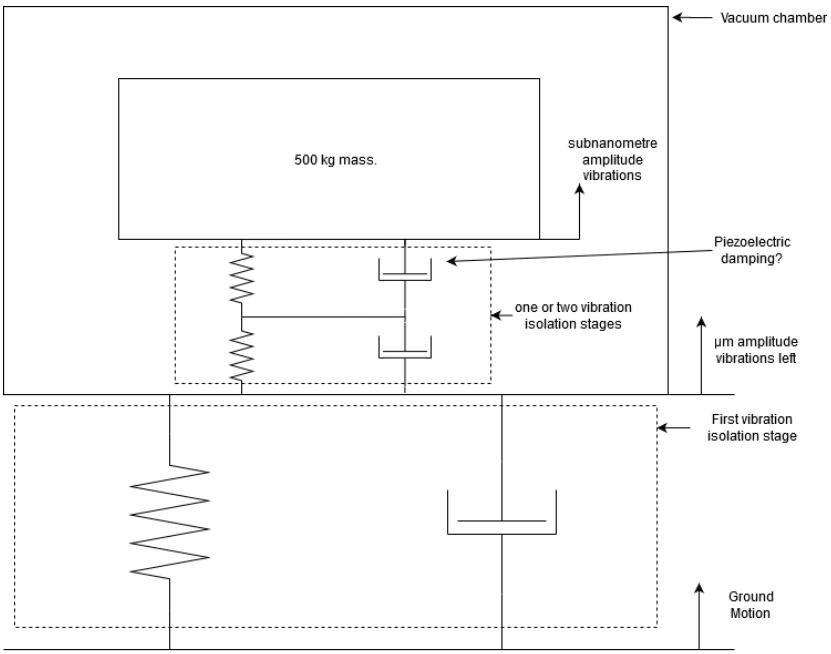

Figure 1.1: A sketch of a possible setup. The ground motion is reduced in the payload using two or three vibration isolation stages. To damp the last stage, which has only (sub)nanometre vibrations, piezoelectric shunt damping could be used.

The aforementioned final vibration isolation needs to have a low resonance frequency due to the nature of passive vibration isolation. In the case of the second (and/or third) vibration isolation stage shown in figure 1.1, the resonance frequency of the system would be around 2 Hz.

Passive vibration isolation is generally achieved by creating a system with a suspension that has a resonance frequency below the unwanted vibrations. All the frequencies that are higher than this resonance will be transmitted through the system with a lower gain (transmissibility), see figure 1.2. At resonance the vibrations need to be reduced by using damping.

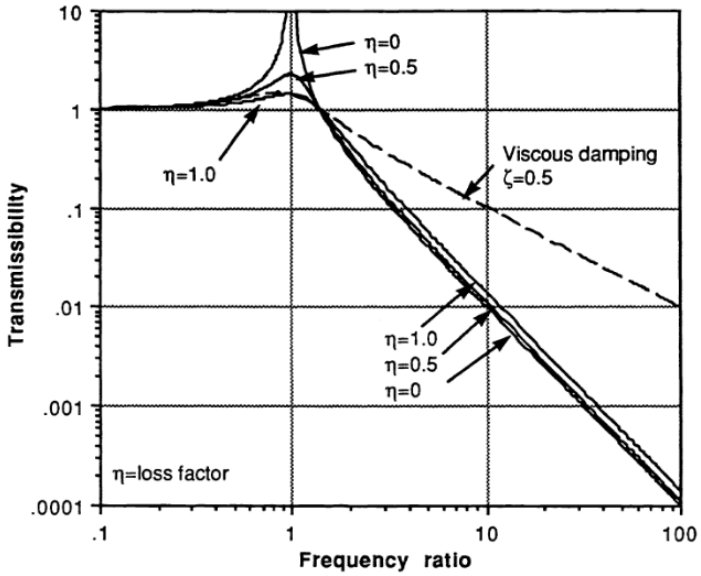

Figure 1.2: Transmissibility graph from a vibration isolation system used by Platus [25]. The transmissibility is the gain at which frequency the vibration is transmitted. It also shows multiple damping lines and that in case of viscous damping, the transmissibility is actually reduced at higher frequencies.

1.2. Objective

This vibration isolation system sparked interest into piezoelectric shunt damping at a low resonance frequency and sub-nanometre amplitude. Piezoelectric shunt damping uses the piezoelectric characteristics of a material to turn mechanical energy (such as vibrations) into electrical energy. This electrical energy passes through a shunt and depending on the type of shunt shows different damping characteristics. A shunt is anything that creates a low resistance path for an electrical current. In the case of piezoelectric shunt damping, the shunt can be passive electrical components such as resistors, inductors, and capacitors.

The ideal situation, in *Settels* eyes, would be to calculate what shunt is required to reach a predetermined damping and simply implement it and forget about it. Ideally, it would have no added controllers or active components. Keep it as simple as possible.

A main research question was formulated: how to attenuate remaining sub-nanometre amplitude vibrations with low frequency using piezoelectric shunt damping? This question was divided into three sub questions.

1. Does piezoelectric shunt damping work at this small amplitude and does damping even work at this small amplitude?
2. How does piezoelectric shunt damping work, what types of shunts are available and what are their advantages and disadvantages?
3. How to add piezoelectric damping to a vibration control system and how to deal with the stiffness of the piezoelectric transducer at a low resonance frequency?

1.3. Structure

In chapter 2 the main and sub questions are researched in the literature, of which a small summary is given. Then in chapter 3 the design of the experimental setup is explained, after which, in chapter 4 some

preliminary results which validate the reduction in ground motion. The piezoelectric shunt damping results will be shown in chapter 5. Subsequently, in chapter 6 the conclusion of the thesis is presented, after which in chapter 7 the thesis and research will be discussed and some recommendations will be given for future research.

2

Background

This chapter explains some basics which will help comprehend the experimental setup and research. First the basic idea of piezoelectric shunt damping and piezoelectricity will be explained. Then some examples of piezoelectric shunt damping and piezoelectric actuators at (sub)nanometre amplitude will be given. Finally, some options for reducing the resonance frequency of a system with the addition of the stiff piezoelectric transducers will be shown.

2.1. Piezoelectric Shunt Damping

Piezoelectric shunt damping was first used by Hagood and von Flotow [12] to reduce vibrations in a cantilever beam. They used a piezoelectric material which was attached to a beam. These patches of piezoelectric material were then shunted using different electrical components such as resistors and inductors.

To explain how this results in damping of the vibrations within the beam, first the direct and converse piezoelectric effect in beams will be explained. Then it will be explained how adding shunts to the patches will result in damping. It is also important to note what previous research was done in piezoelectric shunt damping at nanometre amplitudes. Finally, a few different useful shunts will be shown.

2.1.1. Piezoelectric Equations

Piezoelectric material is created by arranging the dipoles which are within the piezoelectric material [26]. This is done by heating up the material to its Curie temperature and applying an electric field on the material. This will arrange the dipoles along the electric field within the structure as can be seen in figure 2.1.

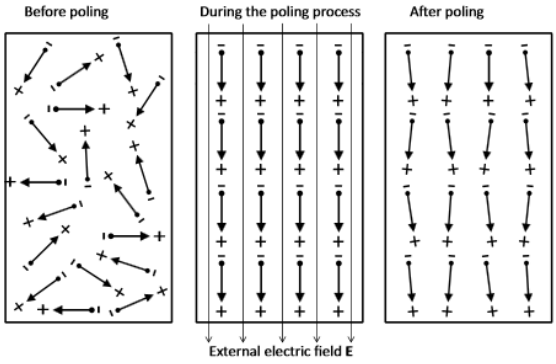

Figure 2.1: Creation of piezoelectric material by heating it up to the Curie temperature and adding a electric field to the material. Figure created by Schmidt et al. [26]

When, after this process, an electric field is applied to the material, the poles will move back to the straight orientation, as is shown in the centre figure in figure 2.1. This will create a strain within the material, this is called the converse piezoelectric effect. Conversely, when a strain is put on the material, the dipoles will move

and will generate a charge flow [18]. These effects are represented in the direct and converse piezoelectric equations, see equation 2.1.

$$\begin{bmatrix} S \\ D \end{bmatrix} = \begin{bmatrix} s^E & d^t \\ d & \epsilon^T \end{bmatrix} \begin{bmatrix} T \\ E \end{bmatrix}. \tag{2.1}$$

Where, S is the strain $[-]$, D is the electric displacement in $\frac{C}{m^2}$, E is the electric field in V/m, T is the stress in Pa, s^E is the compliance in a constant electric field in $\frac{m}{N}$, ϵ^T is the electric permittivity under constant stress in $\frac{F}{m}$, d is the piezoelectric charge constant in C/N and d^t is the transpose of the piezoelectric charge constant when the formula is used in matrix form.

2.1.2. Piezoelectric Shunt Damping

In piezoelectric shunt damping the direct and converse piezoelectric effect in combination with an electrical impedance can be represented as a collocated feedback mechanism [22]. This feedback mechanism is shown in figure 2.2

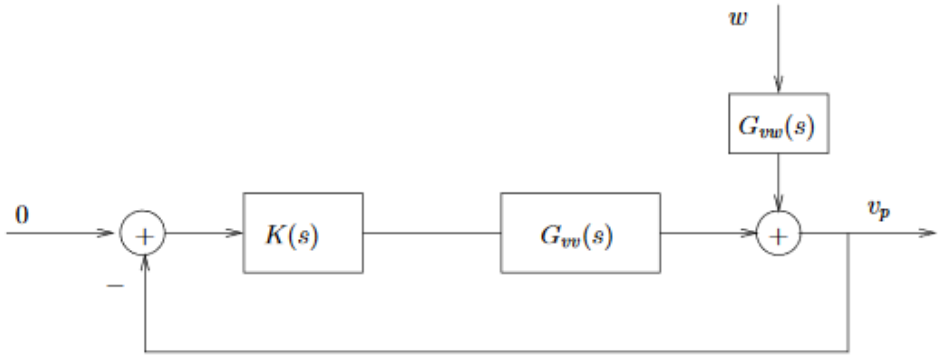

Figure 2.2: Feedback loop of a piezoelectric transducer. Where w is the disturbance, v_p is the voltage over the piezo, G_{vw} is the transfer function from disturbance to v_p, G_{vv} is the collocated transfer function. Figure is from Moheimani et al. [22].

In this thesis the shunts are classified in three ways. Using passive, semi-active or active shunts. Passive shunts use analogue components such as: resistors, inductors, and capacitances. They do not introduce any energy into the system. Semi-active shunts are shunts that also use analogue components, but they do introduce energy into the system. For example, they do this by using op-amps and only do it to create virtual components such as virtual inductors [10]. Finally, there are active shunts. These introduce energy directly into the system. A good example of these use a H_∞, H_2 or LQG controller [8]. These shunts function as the controller $K(s)$ in figure 2.2.

In case of a passive system, the analogue components put an impedance on the electrodes of the piezoelectric material, which results in damping. The impedance ($Z(s)$) creates a controller $K(s)$, which is shown in equation 2.2.

$$Z(s) : K(s) = \frac{sC_pZ(s)}{1 + sC_pZ(s)} \tag{2.2}$$

Where C_p is the capacitance of the piezoelectric material.

2.1.3. (sub) Nanometre Amplitude

The proposed idea in this thesis, is to use piezoelectric shunt damping in structures with nanometre (and ideally sub-nanometre) amplitude vibrations. Thus, it is important to know if piezoelectric shunt damping works at this amplitude. An example of piezoelectric shunt damping in shown in Eielsen and Fleming [5]. In this article, piezoelectric shunt damping is used to increase the accuracy of nanopositioning, by damping the first mode in the system using piezoelectric shunt damping. However, this first mode is at 1.84 kHz, which is couple of orders of magnitudes higher than the wanted 2 Hz.

It is also important to note that in Le Breton et al. [17] they are able to reduce seismic vibrations to sub-nanometre amplitude (0.25 nm RMS) using piezoelectric actuators. The fact that piezoelectric actuators work at sub-nanometre amplitudes indicates that piezoelectric shunt damping might also work at this amplitude.

2.2. Shunt Types

Since in this thesis only two shunts are used, only these will be explained. Other possible shunts and their advantages can be found in my literature study. These shunts described in this thesis are the resistive shunt and the resonant shunt.

2.2.1. Resistive Shunt

Hagood and von Flotow [12] added a resistor to the electrodes of a piezoelectric transducer. The theory being that the strain that is induced in the transducer due to the vibrations, will be converted into electrical energy. This energy will then pass through the resistor and is converted to heat. This conversion results in damping of the system. Optimum damping can be reached by tuning the resistance of the resistor. Hagood and von Flotow [12] calculated an optimal resistance which was extended upon by Neubauer et al. [23]. In Heuss et al. [14] a derivation of the optimal resistance (for the highest damping performance) is used in the system shown in figure 2.3. The resulting equation, which will be used to get the optimal resistance, is shown in equation 2.3.

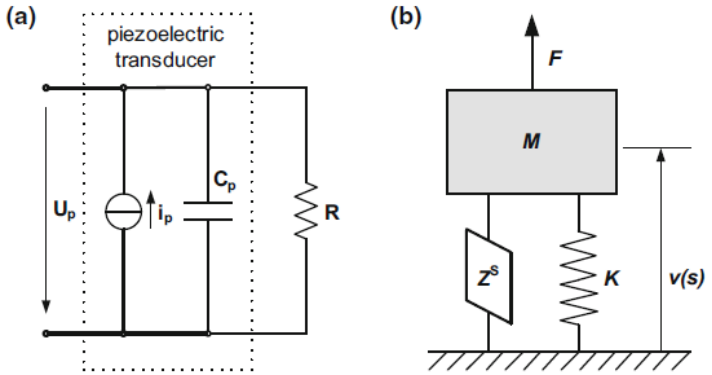

Figure 2.3: These figures shows the electrical model of the transducer when one uses a resistive shunt (a) and it shows the mechanical model (b). The U_p is the voltage in the piezoelectric transducer in V, i_p is the current in the piezoelectric transducer in A, R is the resistance in Ω, Z_s is the piezoelectric transducer with shunt, K is the modal stiffness of the system in N/m, $v(s)$ is the velocity in m/s, F is the force in N and M is the modal mass. The figure is from Heuss et al. [14].

$$R_{R-opt} = \frac{2}{C_{pi}^S \omega_n^E} \sqrt{\frac{1}{4+2K_{ij}^2}}. \tag{2.3}$$

Where R_{R-opt} is the optimal resistance for a resistive shunt in Ω, C_{pi}^S is the capacitance of the piezoelectric transducer with constant stress (clamped) in the ith direction in F, ω_n^E is the resonance frequency of the nth eigen mode with constant electric field in Hz and the equation for K_{ij}^2 is shown in equation 2.4.

$$K_{ij}^2 = \frac{K_{ij}^E}{K+K_{ij}^E} \frac{k_{ij}^2}{1-k_{ij}^2}. \tag{2.4}$$

Where K_{ij}^E is the generalised electromechanical coupling in constant electrical field in N/m and k_{ij}^2 is the electromechanical coupling coefficient.

2.2.2. Resonant Shunt

Hagood and von Flotow [12] then added an inductor in series with the resistor of the piezoelectric transducer and called it a resonant shunt. Due to the capacitance of the piezoelectric transducer, this can be considered as a RLC-circuit. Hagood and von Flotow [12] show that a resonant shunt can be seen as a mechanical vibration absorber, see figure 2.4.

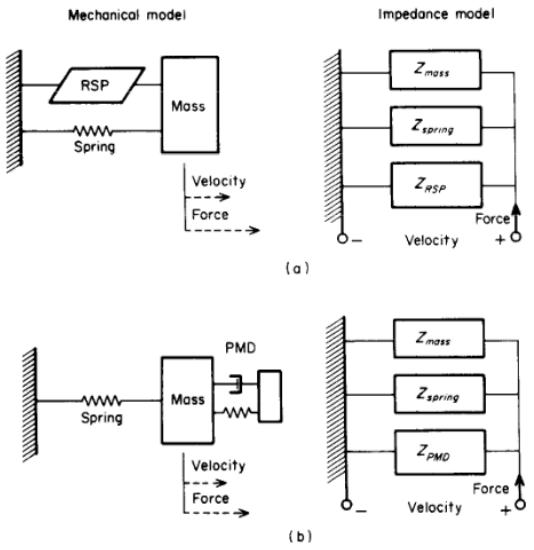

Figure 2.4: (a) shows the RSP (Resonant Shunted Piezoelectric) and (b) shows a PMD (proof mass damper) also known as a mechanical vibration absorber. Figure from Hagood and von Flotow [12].

By tuning resonance of the shunt to the resonance frequency of the mechanical system, the damping performance of the piezoelectric shunt is increased, surpassing the resistive shunt. The optimal resistance and inductance to get the best damping is shown in equation 2.5. This equation is formulated by Heuss et al. [14] and is for the same system as in figure 2.3, except that an inductor is added in series with the resistor.

$$R_{RL-opt} = \frac{2}{C_{pi}^{S}\omega_{n}^{E}}\sqrt{\frac{1}{\frac{2}{K_{ij}^{2}}+4+2K_{ij}^{2}}}.$$
$$L_{RL-opt} = \frac{1}{C_{pi}^{S}(\omega_{n}^{E})^{2}}\frac{1}{1+K_{ij}^{2}}. \tag{2.5}$$

Where R_{RL-opt} is the optimal resistance in a resonant shunt in Ω and L_{RL-opt} is the optimal inductance in a resonant shunt in H.

The resonance shunt has some drawbacks. The first being that for a low frequency, large inductances are needed [13]. The second one is the robustness of the resonance shunt. When the electrical resonance is not correctly tuned to the mechanical resonance, the damping performance is drastically reduced. In practical situations these variations might occur due to environmental conditions and variations in structural load [6]. Variations in the resistance of the shunt have a small effect on the damping performance [24]. The problem lies in the variation of the resonance, and thus in the inductance [24] and the piezoelectric capacitance. An example is shown in Fleming and Reza Moheimani [8]. A 13.5% change in the first mechanical resonance is orchestrated, by adding a mass to the tip of the cantilever beam. The damping performance of the resonance shunt in the first mode is reduced from 14.2 dB to 0.8 dB.

To solve the large inductance problem passively, a capacitor can be added in parallel to the piezoelectric transducer [7]. However, the damping performance of the shunt is reduced. This means that there must be a trade-off between performance and inductance magnitude. In my literature study I could not find passive options to mitigate the degradation of the damping performance due to variations in mechanical resonance.

All of the information given above is in case the resistance and inductance are placed in series. It is also possible to put them in parallel, as was researched by Yamada et al. [28]. They concluded that the resonance circuit in series has a higher damping performance than the system in parallel and that the advantage of the parallel shunt is that it is less susceptible to variation in resistance. This, however, has a small effect [24].

2.2.3. Synthetic Inductors in a Resonant Shunt

To achieve the large inductance in the resonant shunt another option is to mimic a inductor. Basically, by using opamps and passive components one can mimic an inductance which is high enough [10]. Two possible synthetic inductors are shown in figure 2.5. The Antoniou inductor is presented in figure 2.5a. The Antoniou virtual inductor works best, because the Antoniou inductor handles the non-ideal properties of the opamps best [11].

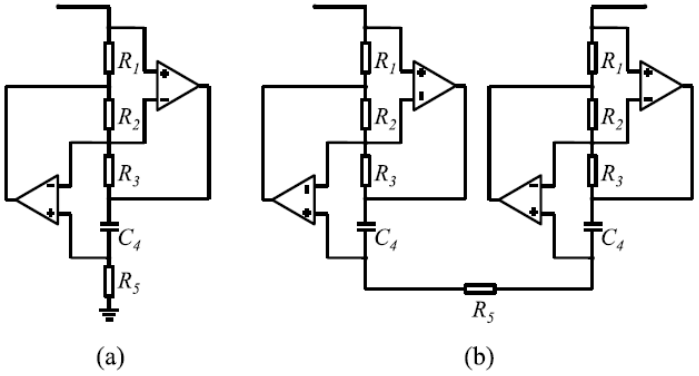

Figure 2.5: Two synthetic inductors. (a) is a grounded inductor and (b) is a floating inductor. Figure from Gripp and Rade [10]

According to Moheimani et al. [22], there are three main disadvantages to synthetic inductors.

1. The first being: "virtual inductors or Riordan Gyrators are difficult to tune and are sensitive to component age, temperature, and non-ideal characteristics."
2. Secondly, due to piezoelectric transducers being able to generate high voltages and due to high-voltage gains created by the circuit, the components need to be high voltage and might be expensive.
3. Finally, multimode piezoelectric shunts need a lot of opamps. For two modes 30 opamps are needed. Generally, you need $2n+4n(n-1)$ opamps. Where n is the number of modes.

2.3. Attachment of Piezoelectric Transducer.

There are three main ways that were found to attach the piezoelectric transducer and to reduce its stiffness: using a mechanical amplifier [1], using a negative stiffness mechanism [3] and using inverted pendulums [25].

2.3.1. Mechanical Amplifier

According to Billon et al. [1], when viscoelastic materials are used to damp these vibration isolation systems, the transmissibility is increased in the higher frequencies. An advantage of piezoelectric damping is that the transmissibility remains low in these frequencies [1], as shown in figure 2.6c.

Billon et al. [1] also created a vibration isolation system using piezoelectric transducer with a negative capacitance and a resistive shunt. This system was created with a mechanical amplifier to reduce the stiffness of the piezoelectric transducer.

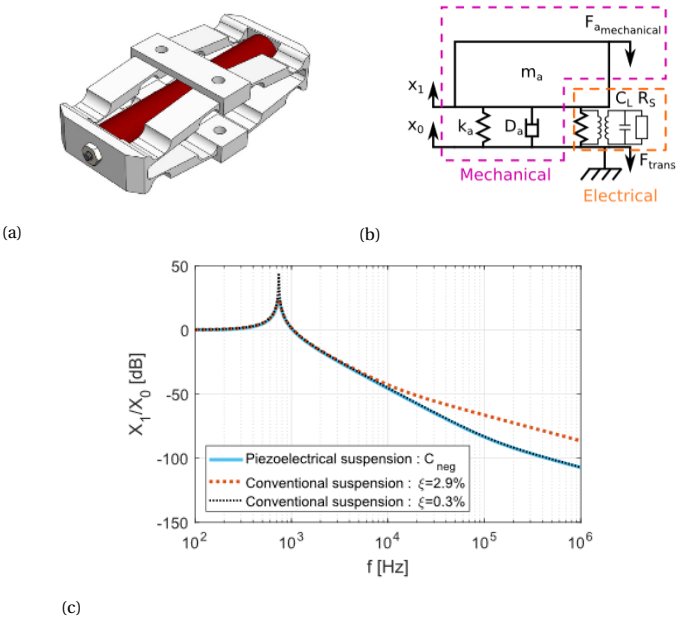

Figure 2.6: In (a) the flextensional piezoelectric transducer can be seen in red. In (b) the piezoelectric transducer with shunt is put in parallel with the mechanical system. Finally, in (c) the transmissibility of the system can be seen. Adapted from Billon et al. [1].

2.3.2. Negative Stiffness Mechanism

Another way to have vibration isolation by having a low resonance frequency, is with a negative stiffness mechanism. Davis and McDowell [3] uses a negative stiffness mechanism as a vibration isolation system and uses a piezoelectric transducer as an energy harvester, see figure 2.7. An energy harvester in this case is basically a resistive shunt, although the resistance can be manipulated to maximize energy harvesting.

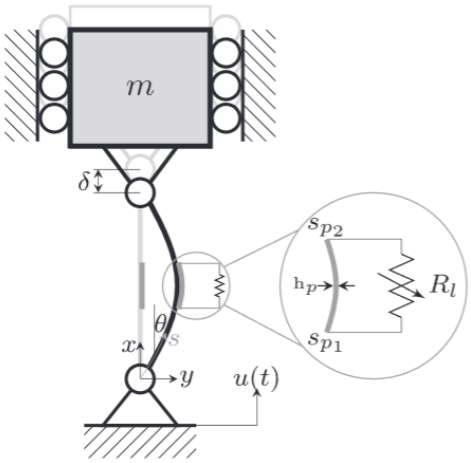

Figure 2.7: A negative stiffness mechanism with a piezoelectric transducer added to it. Its shunt acts as an energy harvester. Figure from Davis and McDowell [3].

2.3.3. Inverted Pendulum

In Platus [25] a vibration isolation system with inverted pendulums for the horizontal isolation and a negative stiffness mechanism for the vertical isolation is used. Piezoelectric transducer patches can be added to the flexures of these systems to create damping. An example of the horizontal system can be found in figure 2.8.

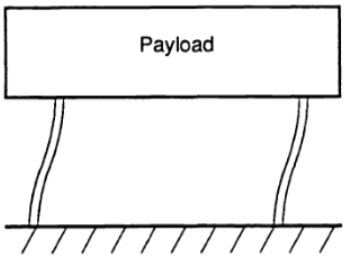

Figure 2.8: An example of a horizontal vibration isolation system. This could be used in combination with piezoelectric transducers to damp the vibrations. Figure is from Platus [25].

However, all these systems would have to be adapted to the piezoelectric transducers when the original resonance frequency is needed. Adding the piezoelectric transducer will affect the stiffness.

2.4. Summary

It was shown that a piezoelectric actuator can actuate at sub-nanometre level amplitudes and that piezoelectric shunt damping works at nanometre amplitude, although in the articles that were found, it was only used at higher frequencies. This indicates that it could work at lower resonance frequencies as well. The basics of piezoelectric shunt damping were explained as well and the two shunts which will be used in this thesis are outlined. Finally, three possible mechanisms to reduce the piezoelectric inherent stiffness were shown.

3

Experimental Setup Design

As was discussed in chapter 2, no examples of piezoelectric shunt damping at sub-nanometre amplitude and with a low resonance are found. Thus, in order to show that this is feasible, a test setup is built. To determine if piezoelectric shunt damping works at (sub)nanometre amplitude, a four step-plan is created:

1. Reduce ground motion in the setup so we are able to measure the damping at the lowest amplitude obtainable with the available hardware.
2. Use a resistive shunt and determine at what amplitude damping still occurs.
3. Increase the sensor resolution to see if sub-nanometre amplitude damping can be achieved.
4. Try different shunts to see how much damping can be achieved.

First a setup needs to be created which can measure the vibrations at the low amplitudes. Since the ground motion will have an effect upon the setup and therefore will give the setup large amplitudes than the wanted (sub)nanometres, there is a need for vibration isolation. A setup which can be adapted to be used is shown first, afterwards calculations will be made to determine the feasibility of the needed ground motion reduction, which will then be validated in chapter four. Then the changes that need to be made to the setup will be explained.

3.1. The "Fine Stage"

The fine stage before it was adapted is shown in figure 3.1. How the fine stage was developed is explained in Joziasse [15]. It has four flexures and before the adaption has a resonance frequency of 2.5 Hz. The setup is actuated using a Lorentz actuator and has a *Renishaw* RLE10 laser encoder, which has a resolution of 10 nm. The setup is operated by a *cRio* from *National Instruments*. The setup was of interest since it has the ability to reduce the stiffness by applying the inverted pendulum effect. Thus, the resonance frequency of the setup can be reduced by either adding mass on top or by reducing the thickness of the flexures.

3.2. Reducing Ground Motion

To reduce ground motion in the setup, multiple platforms were tried with a combination of two vibration isolation tables. The idea being that the best platform can be utilised in the piezoelectric shunt damping experiments. Two types were available in the lab: an active and two passive tables. The passive vibration isolation tables use a low stiffness to reduce the resonance frequency of this table. Due to this low resonance frequency, the higher frequencies have a reduced gain. A problem arises when one wants to use a vibration isolation table and have a setup with low resonance frequency, since vibration isolation tables generally only reduce the ground motion from a certain frequency, see figure 1.2. Thus, if the frequency of the setup is increased, the disturbance of the ground motion can be reduced. After looking at figure 3.2, it was decided to increase the resonance frequency of the experimental setup to 20 Hz. How this was done and more details on the setup is shown in chapter 3.3.

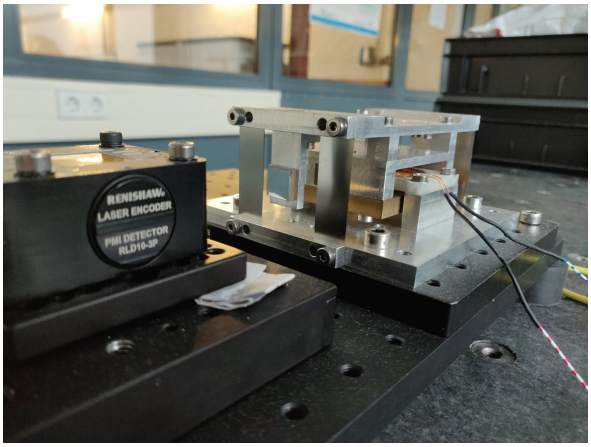

(a) Figure showing the fine stage and the laser encoder.

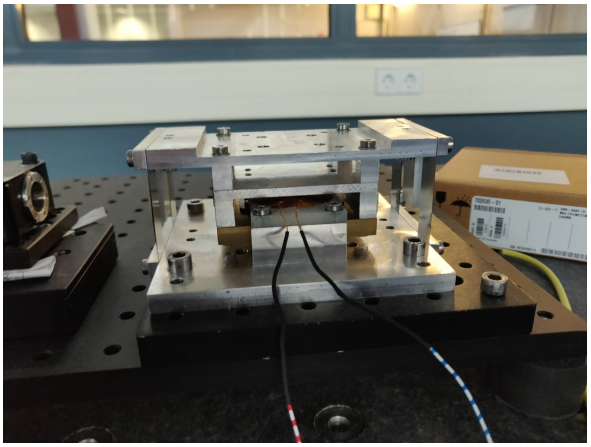

(b) Figure showing a side view of the fine stage.

Figure 3.1: Images of the fine stage in the mechatronics lab before it was adapted. It has a laser encoder to measure disturbance and a Lorentz actuator to actuate the setup.

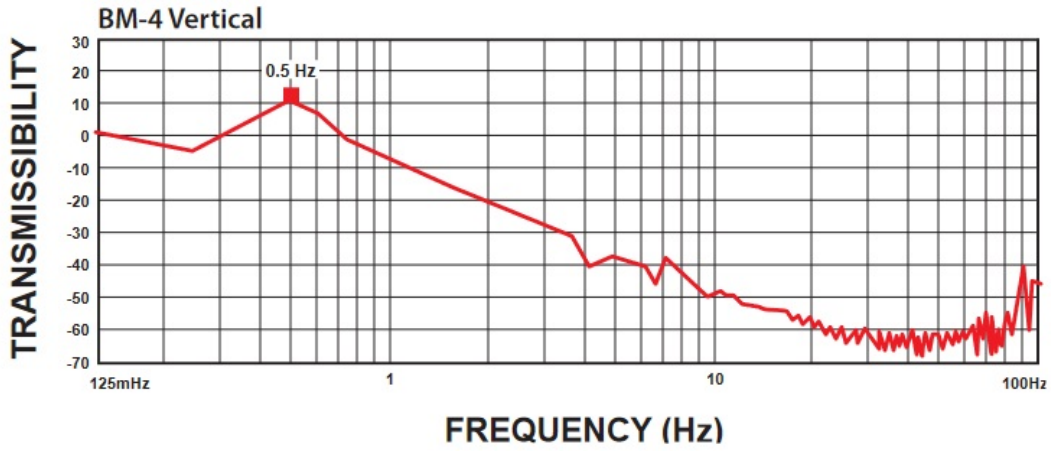

(a) Figure showing the transmissibility of the *MinusK 200BM-4*, with the datasheet in C

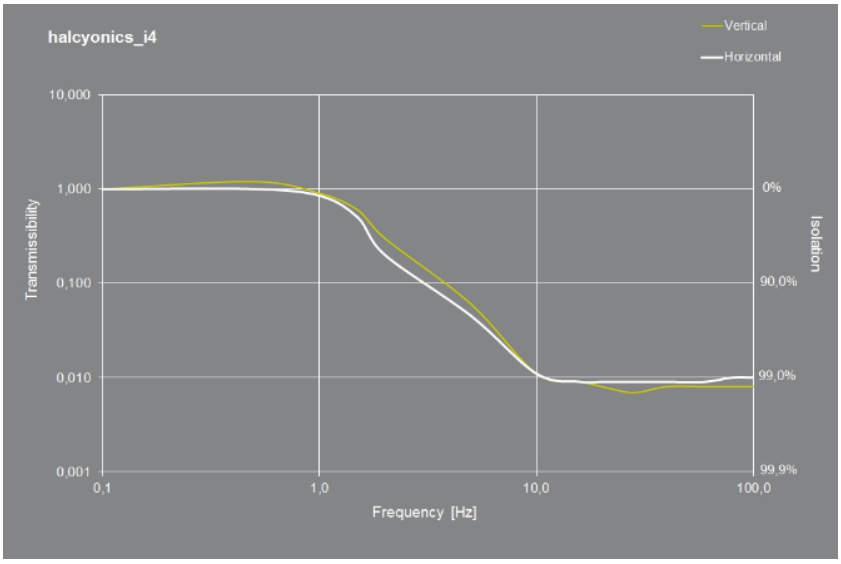

(b) Figure showing the transmissibility of the *Accurion Halcyonics i4*, its data sheet is show in appendix B.

Figure 3.2: The transmissibility curves of two different vibration isolation tables.

To determine what reduction due to vibration isolation can be reached, first a model is created with one passive table. Afterwards, a model is created with two passive tables. It could also be possible to use an active table on top of one passive table, or the other way around. It is important to note that an active table could possibly interfere when small vibrations are measured. This is due to the noise in the motors of active tables. The noise of the accurion i4, which is the available table, is unknown and not shown in its datasheet, see appendix B.

3.2.1. Setup on Passive Table

To determine how much of the ground motion can be reduced using the *200BM-4* passive vibration isolation table (whose characteristics are shown in figure 3.2a), a dynamic model was created. The schematic used for this is shown in figure 3.3. The model is created in one horizontal direction and thus does not take the effects of the other axes into account. A detailed explanation of the model is shown in appendix A.

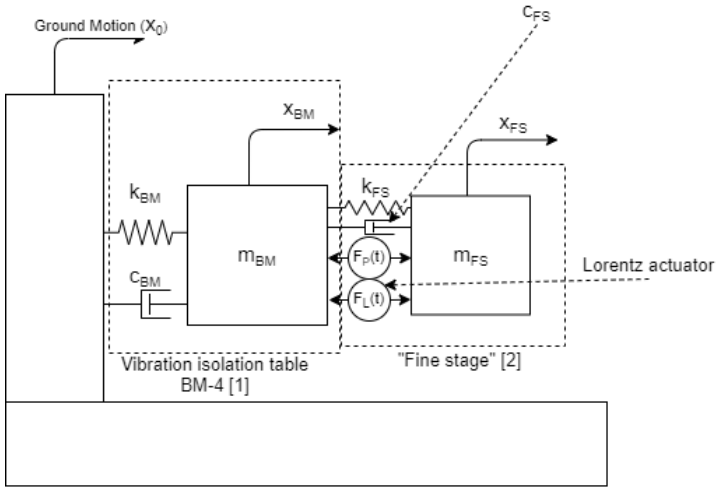

Figure 3.3: Model of the setup on the *BM-4* a passive vibration isolation table from *MinusK*. In this figure, m_{BM} is the mass on top of the passive vibration isolation table without the moving mass of the setup, k_{BM} is the stiffness of the table in $\frac{N}{m}$, c_{BM} is the damping of the table in $\frac{Nm}{s}$, x_{FS} is the position of the payload in m, x_0 is the disturbance due to the ground motion in m, m_{FS} is the top mass of the setup in kg, k_{FS} is the stiffness of the setup in $\frac{N}{m}$, c_{FS} is the damping of the setup without piezoelectric shunt damping in $\frac{Nm}{s}$, x_{FS} is the position of the top mass of the setup in m, $F_p(t)$ is the force on the setup due to piezoelectric shunt damping in N and $F_L(t)$ is the force on the setup due to the lorentz actuator in N.

Using this model a transfer function of the ground motion to the second mass, also known as the transmissibility, can be determined. The calculated transfer function is shown in equation 3.1.

$$T_{onePassive}(s) = \frac{X_{FS}(s)}{X_0(s)} = \frac{0.1235s^2 + 3794s + 1.559 * 10^4}{s^4 + 0.7468s^3 + 1.594 * 10^4 s^2 + 3974s + 1.559 * 10^4} \tag{3.1}$$

Where, $T_{onePassive}$ is the transmissibility of the experimental setup with one passive vibration isolation table, X_{FS} is the Laplace transform of the position of the mass on the fine stage and $X0$ is the Laplace transform of the disturbance of the ground motion.

The resulting transmissibility represented by equation 3.1 can be seen in figure 3.4. This figure shows a reduction of ground motion, with the setup added, of $-32.5\ dB$ at $20\ Hz$. This corresponds to a reduction of 2.37%. The transmissibilty at the resonance of the second mass is dependent on the damping of the experimental setup. A good first guess is to use the same damping ratio as used by Chen [2], since Chen measured this damping ratio preadaptation. However, since the setup will be changed (see chapter 3.3), the only way to know it is by measuring the actual damping.

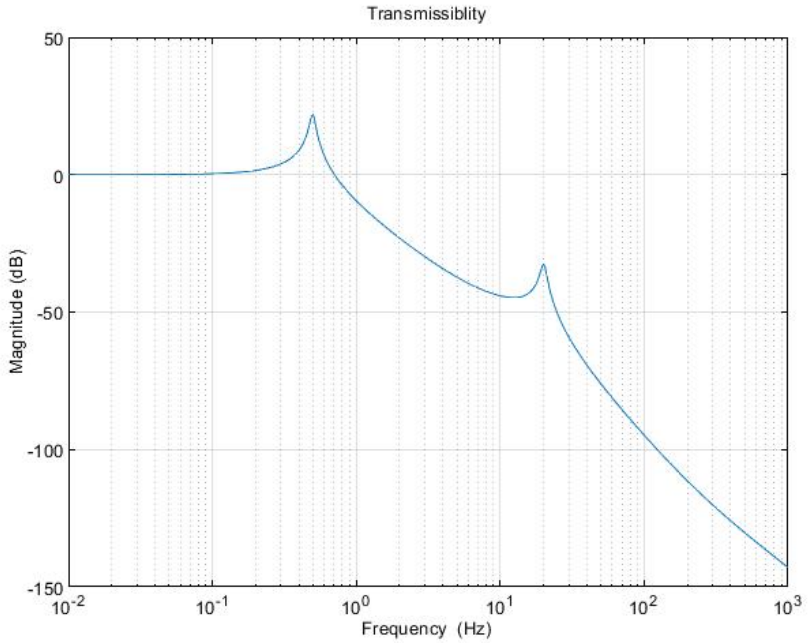

Figure 3.4: This graph shows the transmissibility from ground motion to the experimental setup. This is used to determine the performance of the vibration isolation.

It is also hard to determine what the actual ground motion will be. It either has to be measured using accelerometers/seismometers or by simply receiving the measurements of the setup. To still get an indication of the amplitude of ground motion vibrations, the vibration criteria of *IEST* were used [9]. These criteria were created so buildings can be evaluated for the use of vibration sensitive equipement. Two cases were used, a VC-B floor and an office building floor. They are integrated over their $\frac{1}{3}$ octave band with 20 Hz as middle frequency. The resulting disturbances in μm and the resulting disturbances due to the vibration isolation table are shown in table 3.1.

Table 3.1: The different vibration criteria and their resulting disturbance before and after the vibration isolation table.

Vibration criteria	RMS velocity at 20 Hz	RMS disturbance at 20 Hz	RMS disturbance after vibration isolation at 20 Hz
VC-B floor	25 $\frac{\mu m}{s}$	5.8 μm	0.14 μm
Office floor	400 $\frac{\mu m}{s}$	92 μm	2.2 μm

The RMS disturbance after vibration isolation with its calculated 0.14 μm shown in table 3.1 is larger than the needed nanometres. It is clear that this would not reduce the ground motion enough in either case. Thus, additional vibration isolation is needed.

3.2.2. Setup on Two Passive Tables

Two *MinusK 200BM-4* (see appendix C) are available, which means that by stacking them, more vibration isolation could be achieved. When another passive vibration table of the same type is added, a new three degree of freedom system is created. A model of this system is visualised in figure 3.5. Due to the additional mass spring damper system, vibration isolation will be increased, because there will be a faster declining slope after the second eigenmode. How the dynamic model was calculated can be found in appendix A.

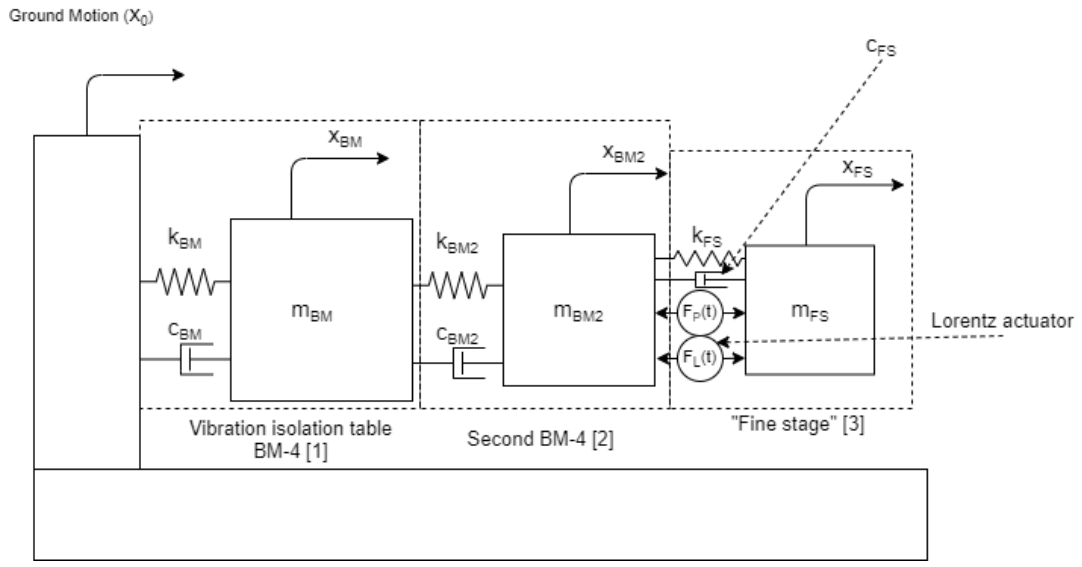

Figure 3.5: Model of the three masses and the vibration isolation tables. In this figure, m_{BM2} is the mass on top of the passive vibration isolation table without the moving mass of the setup in kg, k_{BM2} is the stiffness of the table in $\frac{N}{m}$, c_{BM2} is the damping of the table in $\frac{Nm}{s}$

The calculated transfer function is shown in equation 3.2. This shows the transmissibility of the ground motion to the mass of the actual experimental setup and which results in the graph shown in figure 3.6.

$$T_{TP}(s) = \frac{X_{FS}(s)}{X_0(s)} = \frac{0.1905s^3 + 811.4s^2 + 5.664 * 10^4 s + 9.845 * 10^5}{s^6 + 4.579s^5 + 1.6 * 10^4 s^4 + 1.231 * 10^4 s^3 + 4.159 * 10^5 s^2 + 5.664 * 10^4 s + 9.845 * 10^5} \quad (3.2)$$

Where, T_{TP} is the transmissibility of the experimental setup with two passive vibration isolation tables, and $X0$ is the Laplace transform of the disturbance of the ground motion.

The transmissibility graph shows a reduction in of $-79dB$ at 20 Hz, which corresponds with 0.011 % of the original ground motion. This results in an estimated disturbance in the setup, which can be found in 3.3.

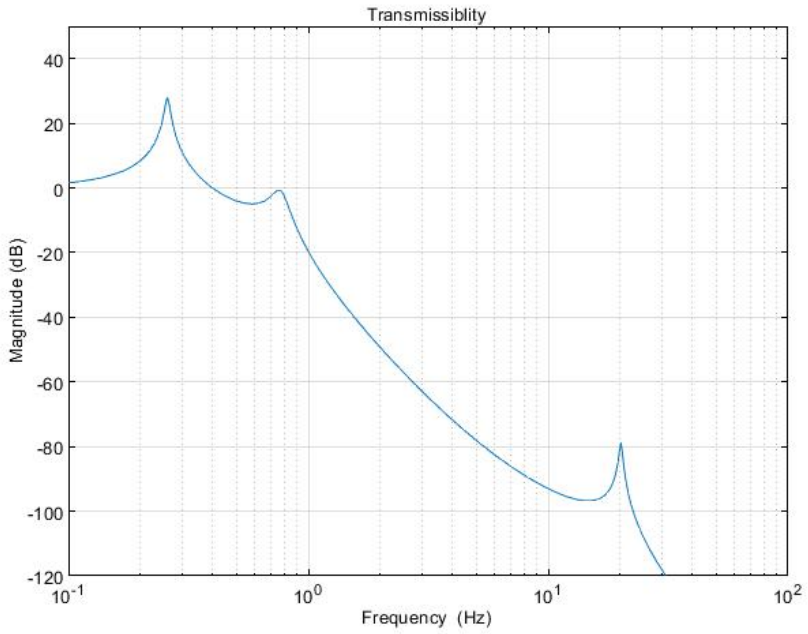

Figure 3.6: this graph shows the transmissibility from ground motion to the experimental setup. This is used to determine the performance of the vibration isolation.

Table 3.2: The different vibration criteria and their resulting disturbance before and after the vibration isolation table. The RMS disturbances are calculated by integrating the RMS velocity across a third of an octave centered around 20 Hz.

Vibration criteria	RMS velocity at 20 Hz	RMS disturbance at 20 Hz	RMS disturbance after vibration isolation at 20 Hz
VC-B floor	25 $\frac{\mu m}{s}$	5.8 μm	0.65 nm
Office floor	400 $\frac{\mu m}{s}$	92 μm	10.4 nm

Since the laser encoder in the experimental setup measures the difference between the setup and the second table and not the exact position of the setup, it is also interesting to see the transmissibility from the ground to what the laser encoder actually measures, which is: $x_{BM2} - x_{FS}$. Figure 3.7 show the transmissibilty. The transfer function for this figure is shown in equation 3.3.

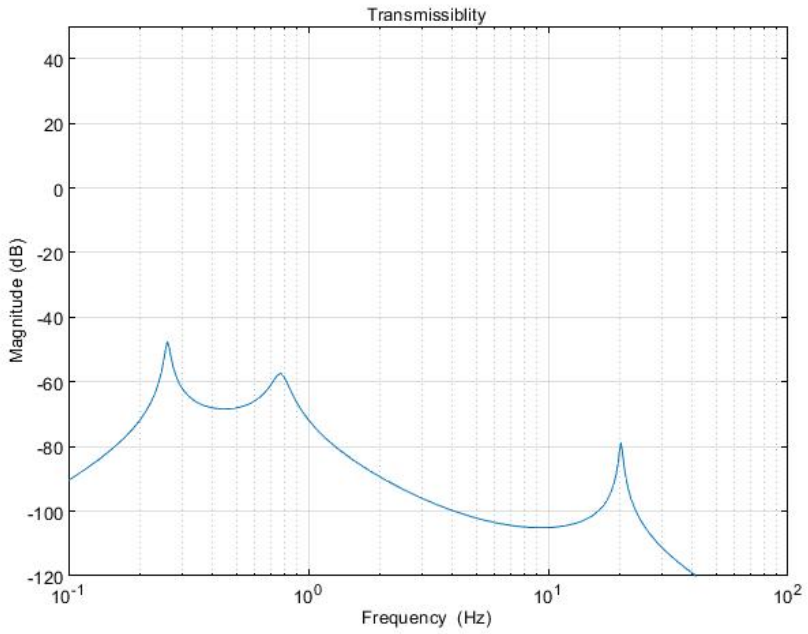

Figure 3.7: this graph shows the transmissibility from ground motion to the laser encoder. This is used to determine the performance of the vibration isolation.

Figure 3.7 shows the same reduction in vibrations as figure 3.6. This means that the position sensor will probably be able to measure the small vibrations induced by the Lorentz actuator and that the vibrations between the two masses are actually small enough to validate if piezoelectric shunt damping damps vibrations at (sub)nanometre amplitude.

$$T_{LE}(s) = \frac{X_{FS}(s) - X_{BM2}(s)}{X_0(s)} = \frac{0.05053s^4 + 3.572s^3 + 62.34s^2 + 2.607 * 10^{-12}s + 1.126 * 10^{-10}}{s^6 + 4.579s^5 + 1.6 * 10^4 s^4 + 1.231 * 10^4 s^3 + 4.159 * 10^5 s^2 + 5.664 * 10^4 s + 9.845 * 10^5} \tag{3.3}$$

Where T_{LE} is the transfer function from the ground motion to what the laser encoder actually measures and X_{BM2} is the laplace transform of the position of the second *BM-4* vibration isolation table.

3.2.3. Setup on Passive and Active Tables

If the setup is placed upon both the *BM-4* (see appendix C) and the *Accurion i4* (see appendix B), it is more difficult to create a transmissibility graph, since the passive dynamics and the characteristics of the active system are unknown. Thus, it is assumed that by using the transmissibility shown in figure B, that the transmissibility can be multiplied with the system. This would mean that with the Accurion an extra 40 dB can be achieved. This corresponds with an additional reduction in ground motion of 1%. Thus a total reduction of -72.5 dB or 0.024% is reached.

Table 3.3: The different vibration criteria and their resulting disturbance before and after the vibration isolation table.

Vibration criteria	RMS velocity at 20 Hz	RMS disturbance at 20 Hz	RMS disturbance after vibration isolation at 20 Hz
VC-B floor	25 $\frac{\mu m}{s}$	5.8 μm	1.4 nm
Office floor	400 $\frac{\mu m}{s}$	92 μm	22 nm

3.3. Adapt the "Fine Stage" Setup

Three adaptions need to be made to use the fine stage to measure piezoelectric shunt damping. The first adaption is to increase its resonance frequency to 20 Hz, this can be achieved by increasing the thickness of

the flexures. The second is to add the piezoelectric patches to the flexures and the final one is to increase the sensor resolution.

3.3.1. Adding Piezoelectric Patches to Setup.

For the stiffness calculation of the flexures in the fine stage, Joziasse [15] uses the equation from Van Eijk [27]. This stiffness calculation is shown in equation 3.4. In this equation the second part on the right is the reduction in stiffness due to the inverted pendulum effect.

$$k_{FS} = 4\frac{12EI}{L^3} - \frac{6mg}{5L} \tag{3.4}$$

Where, E is the Young's modulus of the material of the flexures in Pa, I is the second moment of inertia in m^4, L is the length of the flexures in m, m is the mass which is moving on top, and g is the gravitational constant in $\frac{m}{s^2}$.

To increase the resonance frequency of the fine stage, the thickness of the flexures needs to be increased. The thickness of the flexures was increased to 1 mm and the length of the flexures was increased to 100 mm. Since according to Joziasse [15], the top mass of the fine stage has a mass of 0.57 kg, this results in a resonance frequency of $\frac{1}{2\pi}\sqrt{\frac{k_{FS}}{m_{Fs}}} = 23.7\ Hz$.

This is higher than then the 20 Hz used in the calculations for the vibration isolation. This is in itself not a large problem, since the if the actual setup would have a resonance frequency of 23.7 Hz, it would most likely only result in more vibration isolation. However, the reason that the ground motion calculations done in chapter 3.1 are not changed to 23.7 Hz, is that the actual physical setup has a resonance frequency of 20.3 Hz. Thus, in order to compare the calculated and experimental data, the ground motion calculations were left at 20 Hz.

The inaccuracy between the calculated resonance frequency and the measured frequency might be explained by the fact that Van Eijk [27] states that for thicker leaf springs (0.6 mm), there might be inaccuracy of 5% in the stiffness. When the resonance frequency is recalculated using a stiffness reduced by 5%, a resonance frequency of 16.8 Hz is obtained.

3.3.2. Placement of Piezoelectric Patches

The best location for the piezoelectric patches is on the location which has the highest strain occurs [16]. As is explained in Van Eijk [27], the stiffness of the mechanism (shown in equation 3.4) is calculated by using four mirrored cantilever beams, see figure 3.8. The beams are mirrored around the mirror planes which means that to calculate the stiffness two cantilever beams per flexures are used. The calculation of the highest strain location is done without piezoelectric patch, to simplify the calculation.

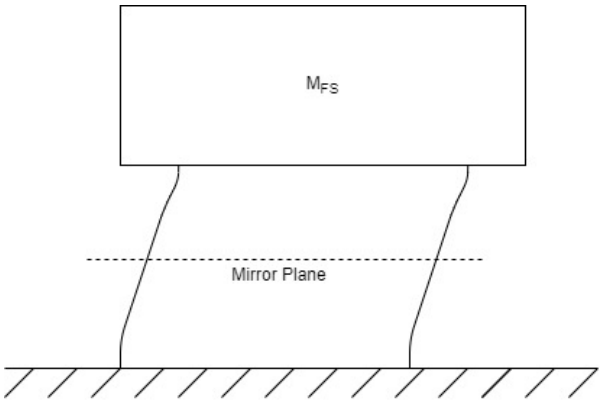

Figure 3.8: Sketch of the "Fine Stage". It shows the side of the fine stage with only two flexures visible. In the figure the mirror plane around which the cantilever beams are mirrored is shown for these two flexures.

By using a distributed parameter system and the Euler-Bernoulli beam theory, the normalised displacement/deflection in a cantilever beam can be determined, which is shown in figure 3.9.

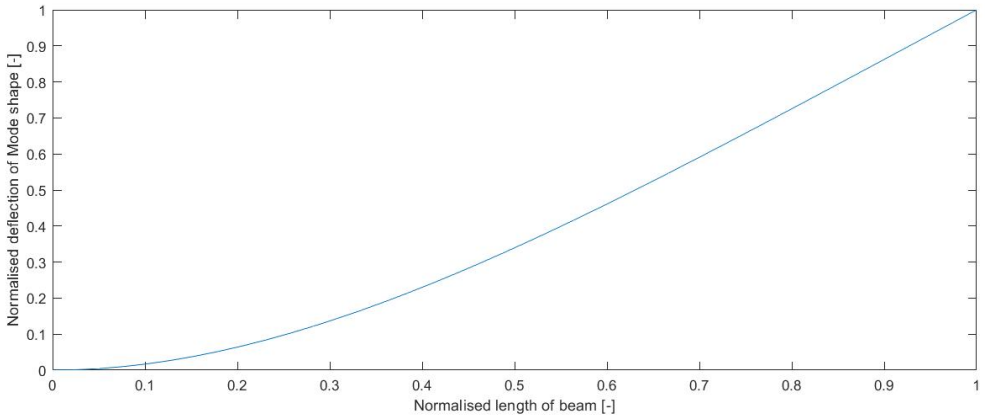

Figure 3.9: This figure show the normalised mode shape of a clamped-free cantilever beam.

Since, the strain energy in the beam can be calculated with the equation in 3.5 and the bending moment is dependent on the curvature of the beam, it is possible to get the best location for the piezoelectric patches.

$$U_{beam} = \int_0^{0.5L} \frac{M^2}{2EI} dx = \int_0^{0.5L} \frac{EI}{2} \kappa^2 dx \tag{3.5}$$

Where, U_{Beam} is the beam strain energy in J, M_{beam} is the mass of the beam in kg and κ is the curvature of the beam.

Taking the second derivative of the mode shape shown in figure 3.9, will yield the curvature of the beam. Then by squaring this as is shown in equation 3.5, the strain energy per length is obtained, see figure 3.10. The figure shows that the highest strain energy is at the beginning of the beam and that the patch should be placed as close to the bottom of the beam (left in the figure) as possible.

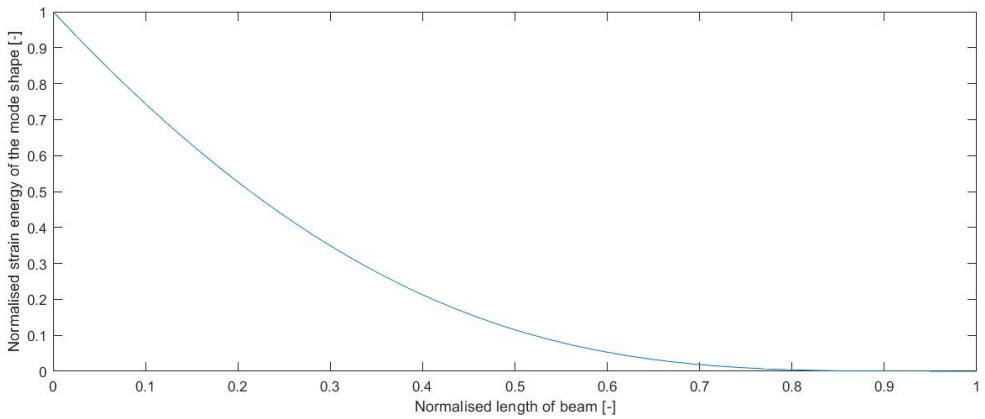

Figure 3.10: This figure gives an indication of the energy per length of the beam. It is calculated by squaring the second derivative (the curvature) of the beam.

Since the piezoelectric patches are only $10x10$ mm, the flexure length is 100 mm, and there is a small Kapton layer in the patches (see figure 3.11), the patch is placed from 0.05 of the normalised length of the beam until 0.25 of the normalised length of the beam. Note that the beam is mirrored and only half the flexure is presented in figures 3.10 and 3.9 and thus the patch will cover 0.2 of the beam. This means that only a part of the maximum strain energy is covered by the piezoelectric patch.

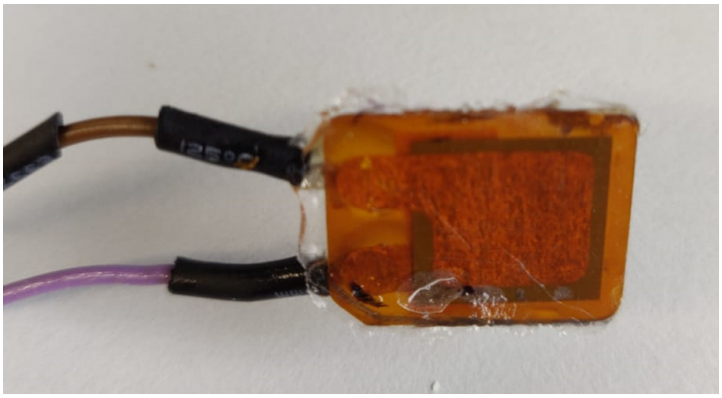

Figure 3.11: Photo of the *P-876.SP1*, which is a piezoelectric patch from *Physike Instrumente*.

Thus, it is expected that the damping performance is reduced. This is also corroborated by Kruik [16], which shows that by increasing the coverage of a beam with constrained layer damping, the damping is increased. This is represented in figure 3.12. since piezoelectric shunt damping and constrained layer damping are both passive damping techniques, it is probable that the same principles hold.

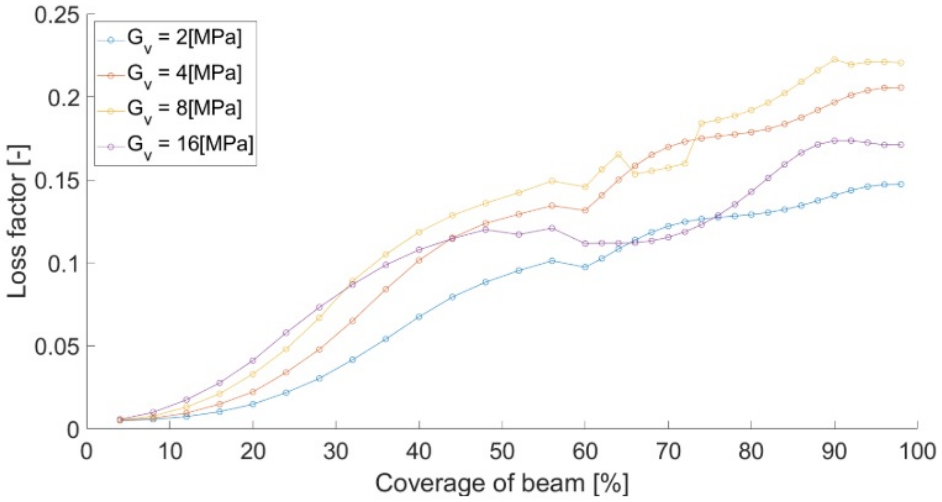

Figure 3.12: This figure shows the loss factor due to damping of constrained layer damping compared to length of the beam covered. This is for the third eigenmode of a cantilever beam, with four different materials used as viscoelastic layer with the constrained layer damping.

Due to this the damping could probably be increased by only increasing the thickness of the flexures. However, the previous findings occurred after construction of the setup, thus the time required to change it was unavailable.

3.4. Sensors

Since the goal of the thesis is to go to sub-nanometre amplitude vibrations, the sensor resolution of the setup needs to be increased. A sensor with a higher resolution is the *PIOne* from *Physike Instrumente*. This sensor has a resolution of $20pm$ and a linearity error of less than 1%. Another candidate is the accelerometer SI1003 from *Colibrys*. When using Zabit et al. [29] it was determined that by using two *SI1003*, with its noise power spectral density, they should be able reach a resolution of 0.9 nm. This is not close to the sub-nanometre resolution that is needed and thus, the *PIOne* is preferred.

3.5. The Resonant Shunt

When using a resonant shunt in piezoelectric shunt damping, the main problem is that it needs a very large inductance. It is shown in chapter 2 how a virtual inductor can be created by using opamps. Since there are

four piezoelectric patches, four resonant shunts have been created using an Antoniou virtual inductor. The circuit used for the resonant shunt is shown in figure 3.13.

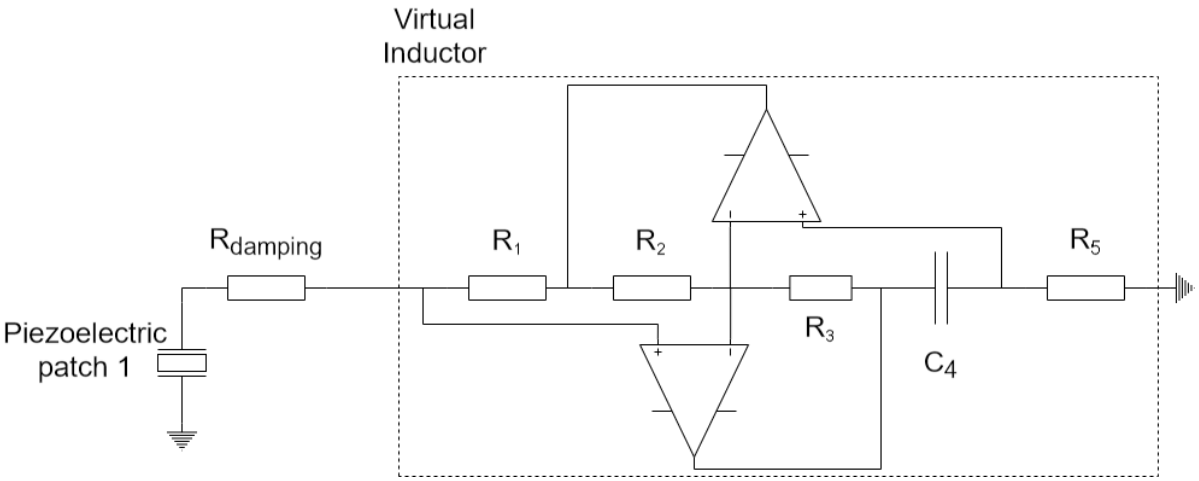

Figure 3.13: In this figure the schematic of one piezoelectric patch and its resonant shunt is displayed. It is powered by a dual power supply with $\pm 16\ V$. The values for the resistors used are: $R_{damping} = 2 * 10^5 \Omega$, $R_1 = 1800\ \Omega$, $R_2 = 120\ \Omega$, $R_3 = 1.1 * 10^4\ \Omega$, $C_4 = 47 * 10^6\ F$, and R_5 is varied in chapter 5 to get the optimal inductance. All resistors are carbon film resistors with a tolerance of 5%. The four capacitors are 35v DC electrolytic capacitors.

A problem with using a virtual inductor is that opamps and resistors have a certain noise. In the case of the used LM324AN, it has a noise power spectral density of 35 $\frac{nV}{\sqrt{Hz}}$ and the resistors have an even higher noise power spectral density of 600 $\frac{nV}{\sqrt{Hz}}$ [21]. This means that if the voltage created by the piezoelectric transducer is lower than this noise, it is likely that no damping is achieved. In this case the resistive and resonant shunt will not be a feasible for the use of piezoelectric shunt damping. Although a solution could be the use of metal film resistors and the passive resonant shunt shown in Lossouarn et al. [20]. Which uses a novel inductor design with a magnetic core.

3.6. Experimental Design

To determine if piezoelectric shunt damping works at nanometre level, first the effect of the ground motion on the system will be checked for the different platforms. These different platforms and their performances will be discussed in the next chapter.

The next step is to see if piezoelectric shunt damping works with only a resistive shunt. This is done by taking two measurements, one with the piezoelectric patches open circuited and one with all the patches connected with the optimal resistance. The setup is actuated at the resonance frequency with the Lorentz actuator and after twenty seconds will let itself damp out. The Lorentz actuator will still be attached, thus the Lorentz actuator will probably be damping the setup as well. That is why the experiments are done in open circuited situation and with resistive shunt. This ensures that the added damping of the resistive shunt can be judged. Then by comparing these measurements in time domain at different amplitude levels, the damping can be obtained. The damping can be calculated by fitting the function shown in 3.6 to the signal and then using the damping ratio in this function.

$$Y = Ae^{-\zeta\omega t} sin(\omega t + \Phi) \tag{3.6}$$

Where, Y is the disturbance of the fitted function in m, A is the amplitude of the vibration in m, ζ is the damping ratio, Φ is the phase difference in rad, ω is the frequency in rad/s and t is the time in s.

Then, by comparing the damping ratios of the open circuited and resistively shunted piezoelectric patches, the added damping due to piezoelectric shunt damping can be determined. The ability to determine the damping can be limited by three things. The first is the resolution of the sensor. If the resolution is not high enough, the damping can not correctly be observed. The second one is the effect of the ground motion. If the

ground motion is larger then the induced vibrations, no damping can be observed either. The third and final limit is if the resistive shunt is not damping anymore.

Finally, it is also interesting to see the level of damping that can be achieved by the resonant shunt and what kind of effect the noise in the opamps and resistors have. The damping of this resonant shunt is measured in the same way as described above.

4

Reduction of Ground Motion

In this chapter, first the experimental setup and its reduction in ground motion will be evaluated. Then the effect of the different configurations of vibration isolation tables upon this ground motion will be appraised. Measurements of the setup with no actuation can be taken to get an indication of the effect of the ground motion on the setup. However, when there is no actuation, other sources of noise such as acoustic noise and sensor noise also have an influence. Thus, when the term ground motion is mentioned, all these sources are considered as well. Four different situations are evaluated. These different situations and their descriptions are shown in table 4.1 for the different setups.

Table 4.1: The different vibration isolation platforms and their description

Platform	Setup Only	Passive	Two Passive	Passive and Active
Description	In this situation only the setup is used and it is placed directly on the granite table.	The setup is place upon a passive *200BM-4* table and the *Accurion i4* active table, but the active vibration isolation is off.	The setup is placed upon two passive *200BM-4* vibration isolation tables.	The setup is on the *200BM-4* and the active *Accurion i4* table with the active vibration isolation on.

4.1. Setup only

To validate the vibration isolation determined in chapter 3, the experimental setup (see figure 4.1) needs to be identified.

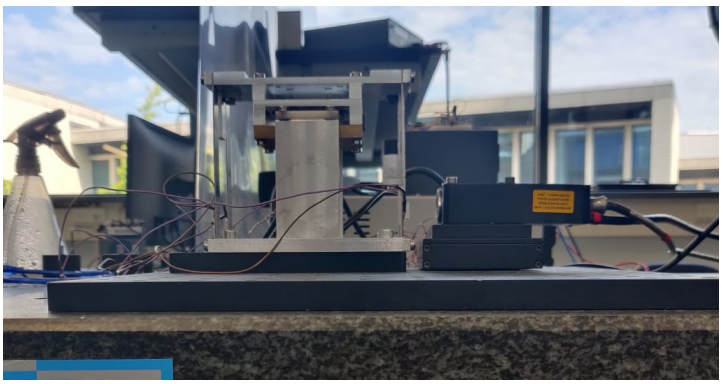

Figure 4.1: This figure shows the experimental setup directly on the granite table.

First the frequency response of the system is determined. This is done by placing the setup on the granite tabletop, leaving the piezoelectric patches open circuited and a chirp signal is sent to the Lorentz actuator. The measured frequency response can be found in figure 4.2. It was created by using the MATLAB function *tfestimate*. The system becomes noisy after around 300 Hz and there appears to be a second mode.

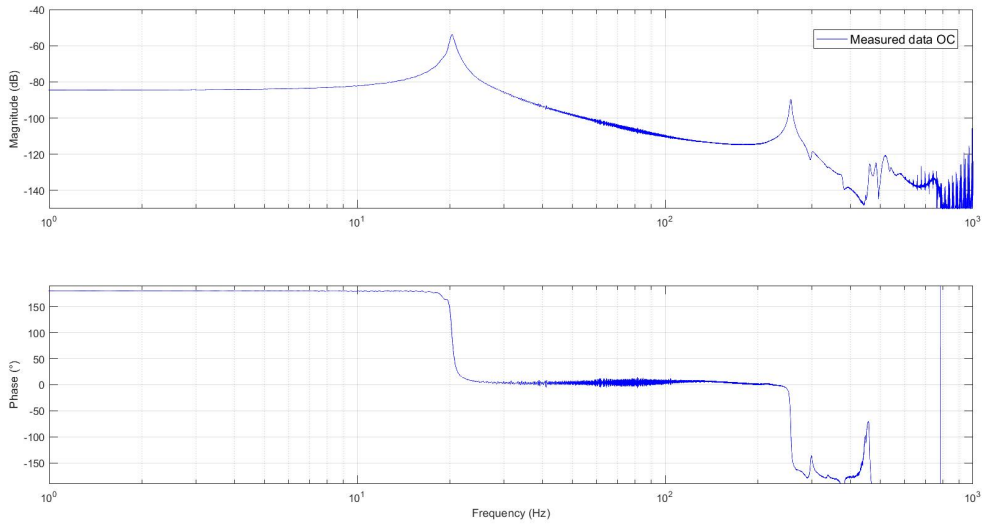

Figure 4.2: In this figure, the magnitude and phase of the measured frequency response of the experimental setup on the granite table are shown.

A second mode can be seen at 256 Hz in figure 4.2. Three theories were formulated as to why. The first: due to the long length of the flexures a second mode of the flexures is seen. The second is that it could be a bending mode because the setup is not actuated halfway along the beams, as is generally done (see Van Eijk [27]). The third one is that: due to the lowering of the mirror of the laser encoder another thicker flexure is created between the mass and the laser encoder. This beam is shown in figure 4.3. The only way to be sure is to research this further and/or doing a FEM analysis. However, since the scope of the research is to see if one mode can be damped at nanometre level, no further research into the second mode has been done.

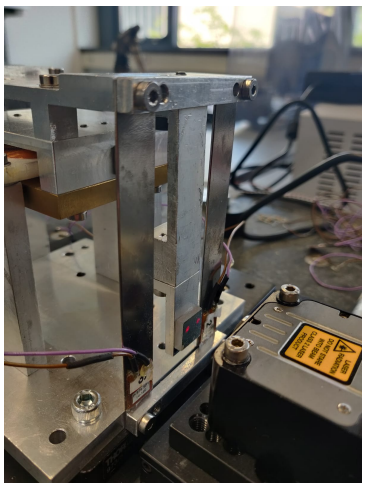

Figure 4.3: The experimental setup is shown with two flexures and an aluminium beam which is in between the flexures. This could be the reason a second mode was detected in the frequency response diagram of the experimental setup.

To determine the effect of the ground motion on the setup, a measurement with the experimental setup on the granite tabletop is taken, see figure 4.1. The Lorentz actuator is not actuating the setup, which ensures that only the ground motion and other background noise is picked up with the laser encoder. The resulting disturbance is shown in 4.4a. Then the power spectral density is taken from this disturbance measurement (see figure 4.4b) to get a better feeling for the different frequencies of the ground motion and their contribution. As can be seen in the cumulative power spectral density and the power spectral density, there is a small peak around 10 Hz. Empirically, it was discovered that this peak appears at seemingly random times. It would be best to use some seismic accelerometers to do further research into the actual seismic vibrations

in the lab.

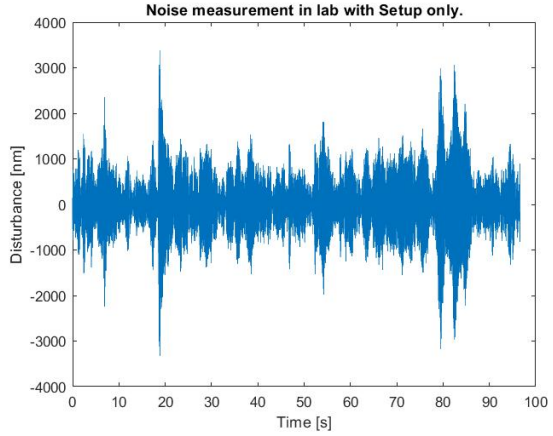

(a) A disturbance measurement of the experimental setup without any vibration isolation and actuation.

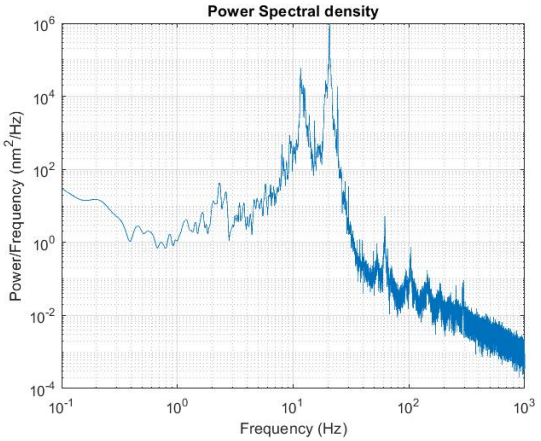

(b) this graph shows the noise power spectral density of the setup.

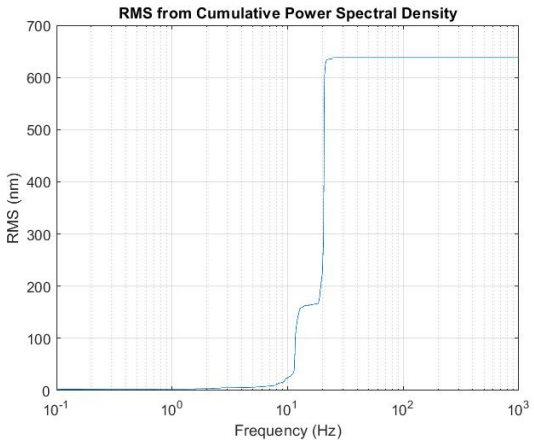

(c) This graph shows the square root of the cumulative power spectral density in nanometres.

Figure 4.4: A measurement taken without actual actuation and/or any vibration isolation. At this point in time it was midday and there were three people in the lab. There was no shunt on the piezoelectric transducers, they were left open circuited.

4.2. Passive

Next the setup is tested in the passive configuration. A photo of the setup with the setup on the passive table is shown in figure 4.5.

The measurement for setup on the one passive table is shown in figure 4.6. It has an RMS error of 94 nm in 1/3rd of the octave band around 20 Hz (The resonance obtained from the power spectral density). By dividing the RMS values of the setup on and off the vibration isolation table, the reduction in vibrations due to the table can be estimated. It results in a reduction of 20 %, the calculated reduction in chapter 3 for one passive table is 2%. It is speculated that this is because the damping ratio from the physical setup is actually lower than the damping ratio which was estimated in chapter 3. Although, it is important to note that the addition of the Accurion i4 in passive mode should add extra vibration isolation. Due to the lack of information of the Accurion i4 in passive mode, it is difficult to compare this situation to either of the calculated situations in chapter 3.

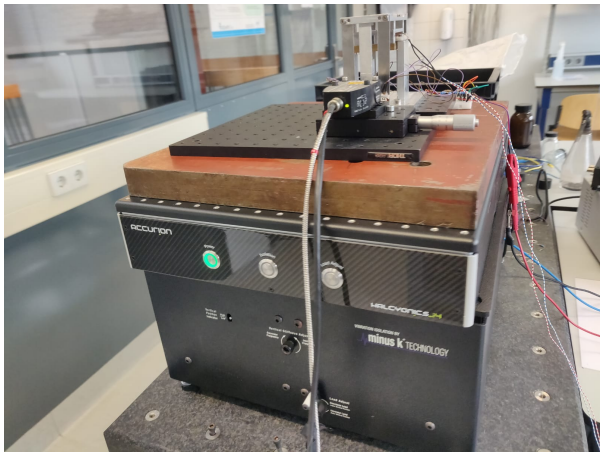

Figure 4.5: This figure shows the experimental setup on the Accurion and the BM-4

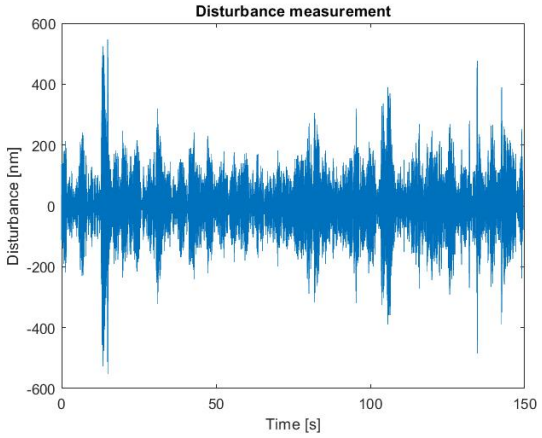

(a) A disturbance measurement of the experimental setup with one passive vibration isolation table and no actuation.

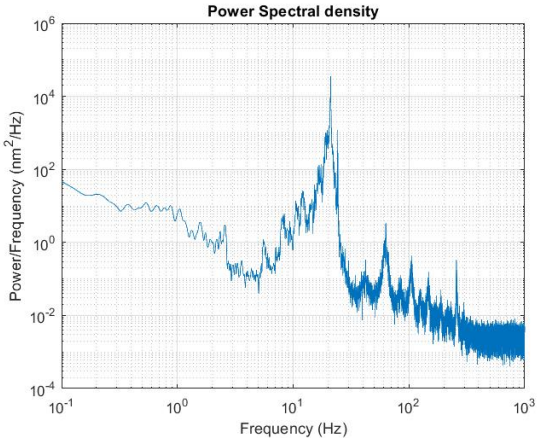

(b) this graph shows the noise power spectral density of the setup on a passive vibration isolation table.

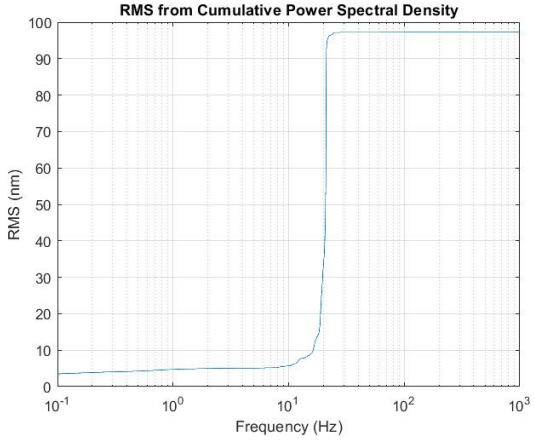

(c) This graph shows the square root of the cumulative power spectral density in nanometres.

Figure 4.6: A measurement taken without actual actuation and/or any vibration isolation. At this point in time it was midday and there were three people in the lab. There was no shunt on the piezoelectric transducers, they were left open circuited.

4.3. Two Passive tables

In figure 4.8, the results for the two passive vibration isolation tables stacked upon each other are shown. A photo of the setup is shown in figure 4.7.

Figure 4.7: This figure shows the experimental setup on the two passive *200BM-4* vibration isolation tables.

The surprising part about figure 4.8, is that it appears that the vibration isolation is even worse than the passive platform. It was speculated that this was due too two reasons. The first being that because the maximum payload of the *MinusK 200BM-4* is 92 kg and its minimum payload is 63 kg (see appendix C), the second vibration table does not work as it should. Since total mass on the first vibration isolation table is (in order): the second table (32 kg), a 50 kg steel mass and then the setup of 5 kg. This means that the total mass on the first table is 87 kg, while on the second table the total mass is only 55 kg. That is why the second table is below its minimum payload and the vertical spring is actually pushing the mass all the way to the top. This ensures that the payload is actually not "floating", but pushed against its maximum and thus will probably transfer the vertical vibrations. The second reason could be that in the passive platform setup, the active table in passive mode is actually adding additional vibration isolation. At least it can be concluded that, two passive table stacked upon each other, in its current configuration, will not be usable in the piezoelectric shunt damping experiment.

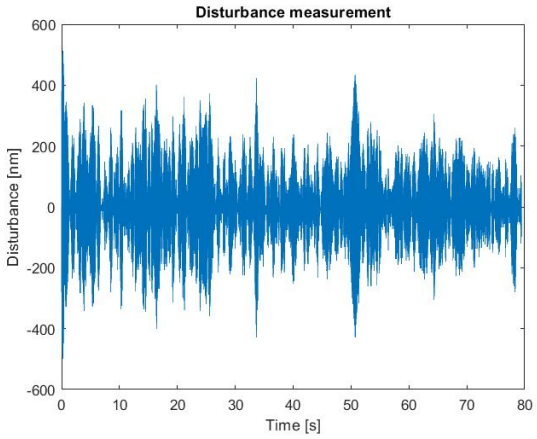

(a) A disturbance measurement of the experimental setup with two passive vibration isolation tables and no actuation.

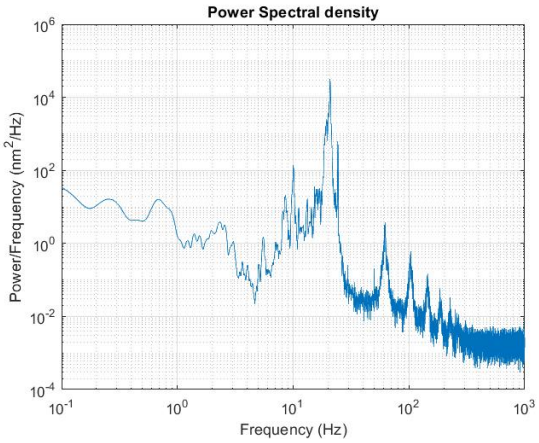

(b) this graph shows the noise power spectral density of the setup on two passive vibration isolation tables.

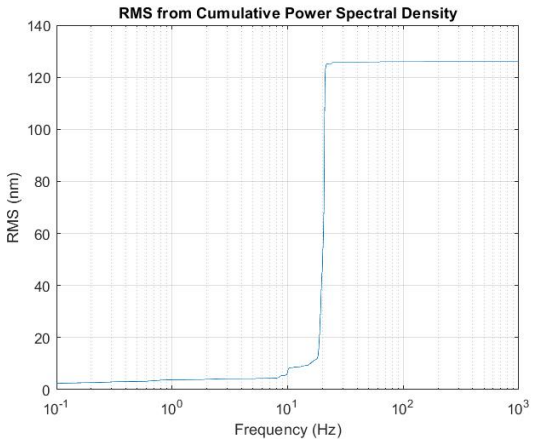

(c) This graph shows the square root of the cumulative power spectral density in nanometres.

Figure 4.8: A measurement taken with two passive vibration isolation tables stacked upon each other and no actuation. There was no shunt on the piezoelectric transducers, they were left open circuited.

4.4. Passive and Active

The measurement for the setup on an active and passive vibration isolation table is shown in figure 4.9 and its physical setup is the same as in figure 4.5, except that the active vibration isolation is turned on. It has an RMS ground motion value of 16.4 nm. The RMS ground motion within the 1/3 octave band around the 20 Hz is 11 nm. This is promising for the ability to measure piezoelectric shunt damping at around 100 nm. In figures 4.9b and 4.9c, it appears that there is more power, and more RMS disturbance at the lower frequencies. It is speculated that the small peak around 0.6 Hz is due to the eigenmode of the first mass, which should be visible according to figure 3.7. The mode of the active vibration table is not visible, since, as can be seen in figure 4.4, there is no increase in gain at the resonance of the *Accurion*.

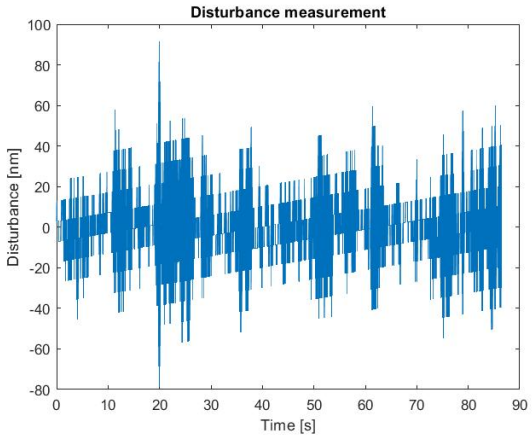

(a) A disturbance measurement of the experimental setup with one active and one passive vibration isolation tables and no actuation.

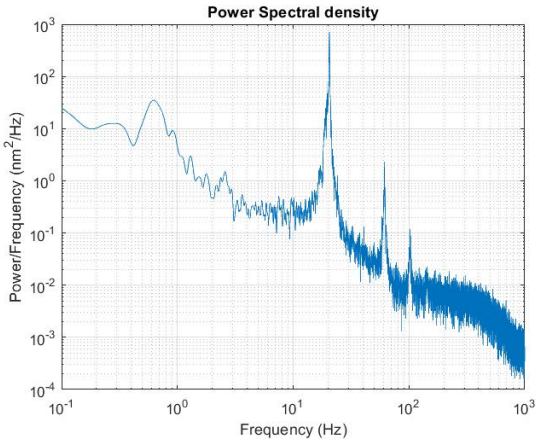

(b) This graph shows the noise power spectral density of the setup on one active and one passive vibration isolation tables.

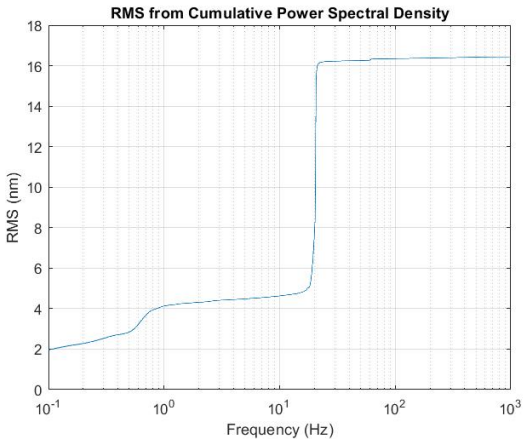

(c) This graph shows the square root of the cumulative power spectral density in nanometres.

Figure 4.9: A measurement taken without actual actuation and with an active and passive vibration isolation table. There was no shunt on the piezoelectric transducers, they were left open circuited.

4.5. Conclusion

When the calculated and measured vibration isolation are compared, it appears that the actual vibrations in the lab are quite similar, but lower than the office floor *IEST* criteria. When the passive and active platform is compared, the calculated performance for the office floor was 22 nm RMS, while in actuality a RMS of 11 nm around 20 Hz was reached. However, what can be concluded from these different setups is that the only viable candidate (at this time) is the passive and active configuration. Since the RMS noise value is 16.4 nm, it is concluded that no sub-nanometre measurements can be done using this configuration and that only measurements in the nanometre range can be done.

5

Results of Piezoelectric Shunt Damping

To determine if piezoelectric shunt damping works at nanometre amplitude, two different shunts are used. These are: the resistive shunt and the resonant shunt. According to the literature (see chapter 2), the resonant shunt should surpass the resistive shunt in damping performance. First the optimal resistance for the resistive shunt is experimentally determined at large amplitude (around $6 * 10^4$ nm). Then a resonant shunt is tried, it is hypothesised that at lower amplitude more damping helps discern the differences between the measurements.

5.1. Resistive Shunt

First the resistive shunt was tested. Different resistances were tried to evaluate at what resistance highest damping performance is achieved. Although all resistances damp up to a point, there is an optimal resistance at which the damping performance is highest [19]. To determine the different damping values of the resistances, the step response of the system with the different resistances is measured. Then by using a function fit with equation 3.6 as the function, the different damping ratios were calculated. All the measurements in this section are a step response, of which the offset is removed. This is done by only using the data after the step and then by shifting the data by removing the arithmetic mean of this data. In this case the setup is also on top of the passive and active platform, which is described in chapter 4. The resulting fitting parameters and their respective resistances are shown in table 5.1.

Table 5.1: The different resistances and their fitted parameters. Which can be used to determine to optimal resistive shunt.

Resistance (Ω)	$0.7 * 10^6$	$1 * 10^6$	$1.1 * 10^6$	$1.2 * 10^6$	$1.7 * 10^6$
Resonance frequency (Hz)	20.24	20.28	20.23	20.23	20.26
Phase shift (rad)	-1.412	-1.303	-0.8745	1.439	2.491
Amplitude (nm)	$5.965*10^4$	$6.016*10^4$	$6.07*10^4$	$5.977*10^4$	$6.01*10^4$
Damping ratio	0.0032	0.0034	0.0036	0.0035	0.0033
NRMSE of the function fit	0.05	0.07	0.05	0.05	0.05

Table 5.1 shows that the optimal resistive shunt is $1.1 * 10^6$ Ω. However, this is dependent on how well the function fits. To show how well the function fits, the Normalised Root Mean Square Error (NRMSE) is also calculated. The NRMSE of every fit is shown in the last row of table 5.1. The closer the NRMSE is to 0, the better the fit. In figure 5.1, the fit accuracy is shown by plotting the fit and the measured data together.

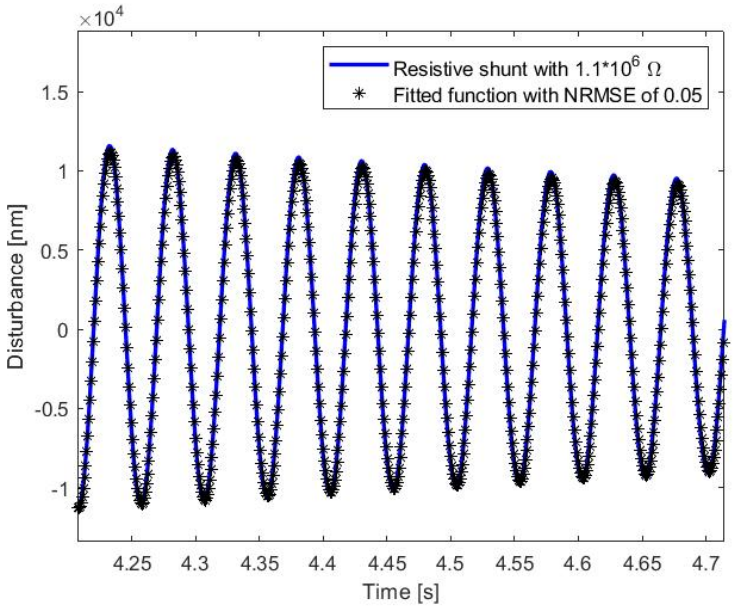

Figure 5.1: A part of the measured disturbance of the step response function of the $1.1 * 10^6$ resistive shunt and its fitted function are shown. The fitted function seems to follow the measured very well.

Figure 5.1 shows that the fit with an NRMSE of 0.05 follows the output very well. In Figure 5.2, the optimal resistive shunt is shown versus the open circuited damping. The dotted line represents the damping line of the system, which is calculated using $Ae^{-\zeta\omega t}$. This is done using equation 3.6 and the fitted resonance frequency and damping ratio. At this amplitude the resistive shunt is clearly damping, although it has a low damping performance.

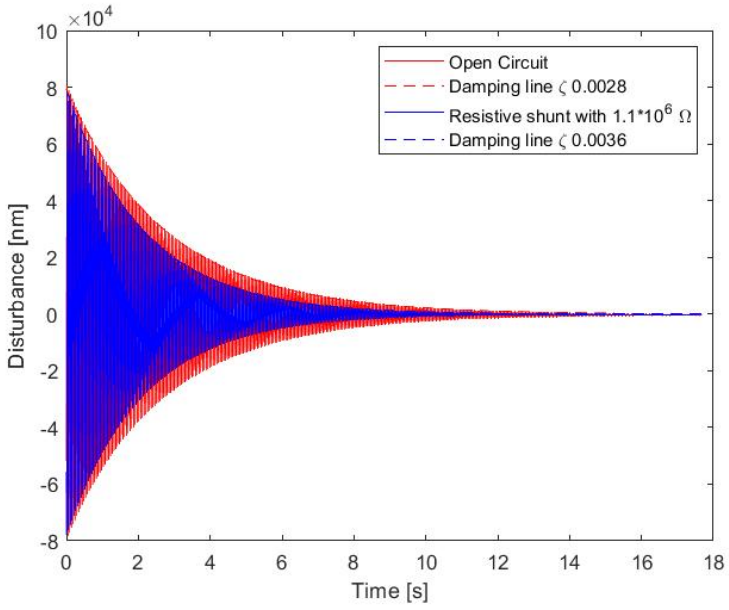

Figure 5.2: In this graph, the step response with all piezoelectric transducers open circuited vs all transducers with the experimentally determined optimal resistive shunt is shown. The offset of these measurements are removed, by only using the data after the step and removing the mathematical mean of the data.

5.1.1. At Reduced Amplitude

Now that the optimal resistance is determined, the amplitude can be reduced too see at what level it either: has to much disruption due to ground motion, is not damping anymore, or the resolution of the linear en-

coder is not good enough. To determine at what amplitude there is damping, the measurements are shifted along the x-axis until they start at the same amplitude of 250 nm and then the mean of the data is removed to remove the offset. An example is shown in figure 5.3, where the measurements from figure 5.2 are shifted along the x-axis until both start with an amplitude of 250 nm.

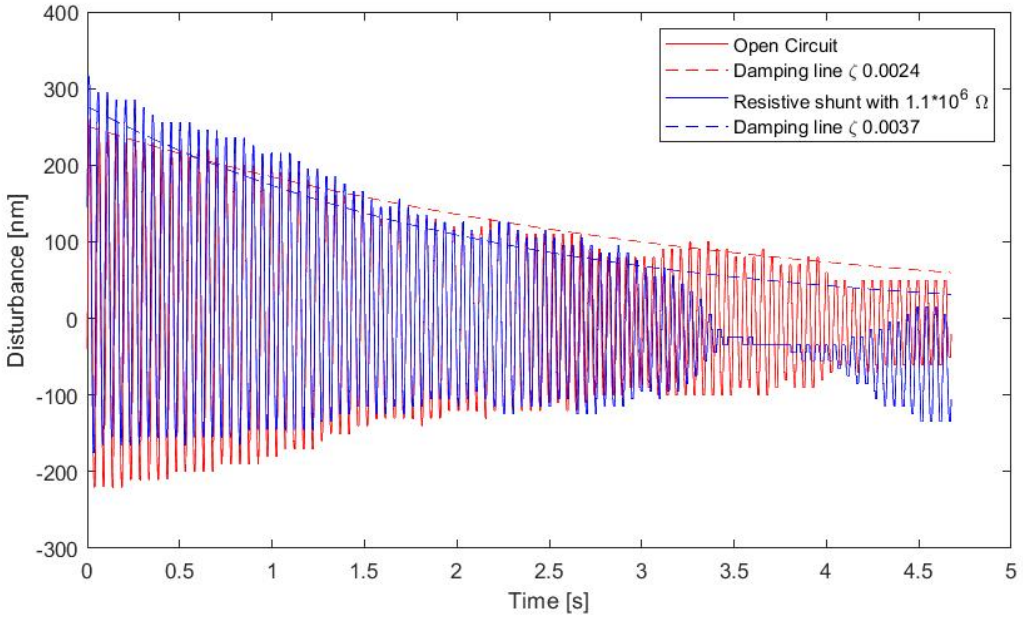

Figure 5.3: The measurements of figure 5.2 are shifted along the y and x axis so the mean of the disturbance is put on the zero of the y-axis and the x-axis is shifted so the amplitudes are around 250 nm. A trend downwards can be seen within the figure.

The figure shows a small trend downwards. This is probably due to the Lorentz actuator of the setup not being able to hold the position of the step response and moving slowly back due tot the force of the flexures. Thus, to be able to compare the measurements at low amplitude, the input signal is changed. Instead of a step response as input signal, the Lorentz actuator was given a 20 seconds sine wave input signal with the open circuited resonance frequency of the system. Then the setup was left to damp itself out. These measurements can then be compared at different amplitudes with the same steps as described above.

To determine if the resistive shunt damps at 250 nm, ten measurements were taken with the steps explained above. Five are open circuited and five are with the optimal resistive shunt. Figure 5.4 shows the two best and the two worst combinations of the ten resistive shunt measurements at 250 nm, according to the NRMSE.

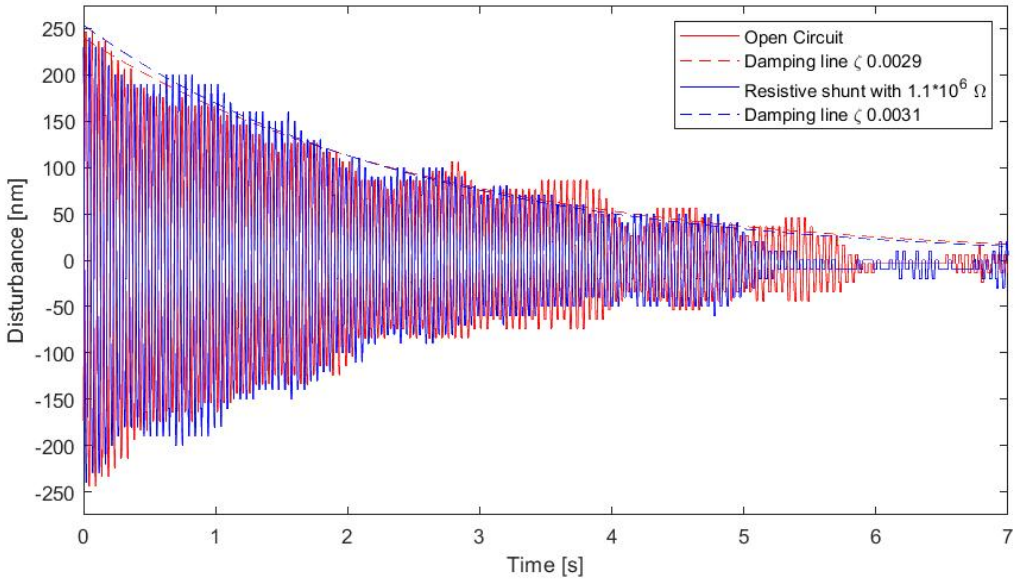

(a) This figure shows a combination of the two best measurements starting amplitude of around 250 nm. Both measurements shown have a NRMSE of 0.17.

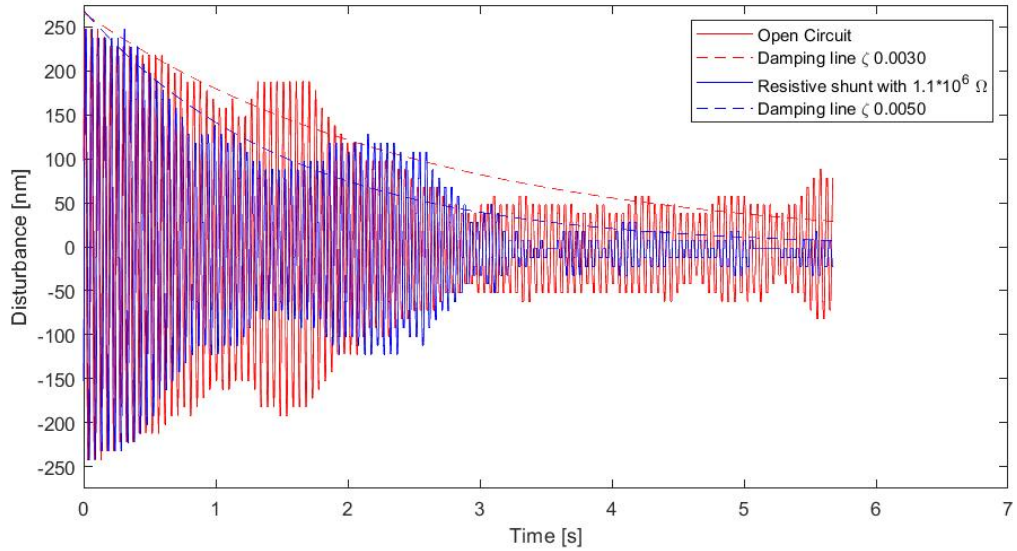

(b) This figure shows a combination of the two worst measurements starting amplitude of around 250 nm. The open circuited measurement has a NRMSE of 0.38 and the resistive shunt has an NRMSE of 0.36.

Figure 5.4: Ten measurements at an amplitude of 250 nm. In five measurements the piezoelectric patches are open circuited and in five measurements they have a resonant shunt. They are compared in two figures where the best and the worst of the five are compared.

Even when one only looks at the best situation as shown in figure 5.4a there is no clear difference in damping at 250 nm. Do note that the day these measurements were taken, it was very busy in the building and this causes a lot of ground motion. It was hypothesised that when larger damping is achieved by using a resonant shunt, a better and clearer distinction between damping can be found at these lower amplitudes.

5.2. Resonant Shunt

the next step is to check the damping performance of the resonant shunt. The damping performance of the resonant shunt was evaluated for two reasons: The increase in damping might show the damping clearer at low amplitude when the ground motion is disturbing the measurement and to see what the performance is compared to the resistive shunt. The layout for one of the four resonant shunts is shown in figure 3.13. By

changing the resistor values the inductance in this virtual circuit can be adjusted. Since all resistances are carbon film resistors with a tolerance of ±5%, the accuracy of the virtual inductance value will be diminished. The optimal inductance was experimentally determined by varying the resistor R_5 and by keeping the other resistors and the capacitor the same.

5.2.1. Optimal Inductance

The optimal inductance was determined in a different way than for the resistive shunt. The test was done on the two passive platform instead of on the active platform (as explained in chapter 4). Another difference is that the measurement did not have a step as input, but the setup was actuated for 20 seconds on its resonance frequency. It is important to note that on the two passive platform, the resonance frequency of the setup was found to be 20.7 Hz, which is higher than the resonance frequency when the setup is placed on the active platform. This is probably due to the dynamics of the different platforms. In table A.1 the fitting parameters and the NRMSE are shown.

Table 5.2: The different virtual inductances and their fitted parameters.

R_5 (Ω)	840	1050	1400	1500	1600	2000
L (H)	6500	8100	11000	11600	12400	15500
Resonance frequency (Hz)	20.5	20.5	20.7	20.6	20.7	20.6
Phase shift (rad)	0.84	-2.7	-1.6	-2.0	-2.9	0.14
Amplitude (nm)	1.46e+05	1.49e+05	1.5e+05	1.53e+05	1.52e+05	1.5e+05
Damping ratio	0.0068	0.0084	0.0095	0.010	0.0097	0.0068
NRMSE of the function fit.	0.06	0.062	0.024	0.034	0.038	0.06

It is clear from this table that the best highest damping ratio is obtained when using a R_5 = 1500, which is why it will be used in the following measurements. It is important to note that there are two caveats. The first is that the resonance frequency of the open circuited setup on the two passive platform is higher (20.7 Hz vs 20.3 Hz) than the resonance frequency of the setup on top of the active platform. This means that the resonant shunt might be mistuned. Although, in the following subsection a similar damping performance is achieved. The second caveat is that for the damping resistor $R_{damping}$ (see figure 3.13) in the resonant shunt, no optimal value is experimentally validated. The implemented resistance of $2 * 10^5$ Ω is the resistance which was calculated using equation 2.5. Note that according to Niederberger et al. [24], the resonant shunt has less damping performance degradation due to a variation in damping resistor.

5.2.2. Comparison at 250 Nanometre Amplitude

After the optimal inductance was determined, the performance at the lower amplitudes is evaluated. Four measurements were taken with resonant shunt and four measurements were taken with the piezoelectric patches in open circuit. These were taken in quick succession alternating the open circuited and resonant shunt measurement. The damping performance is checked at different amplitudes. The first check is at 250 nm. The measurements are shifted so they start and overlap at 250 nm and are shifted so their mean disturbances are zero. The resulting figures are shown in figure 5.5, where figure 5.5a shows the open circuited measurements and figure 5.5b shows the resonant shunt measurements. The damping lines presented here are determined by taking the absolute of the measurement and fitting the function $Ae^{-\zeta\omega t}$ to the measurement.

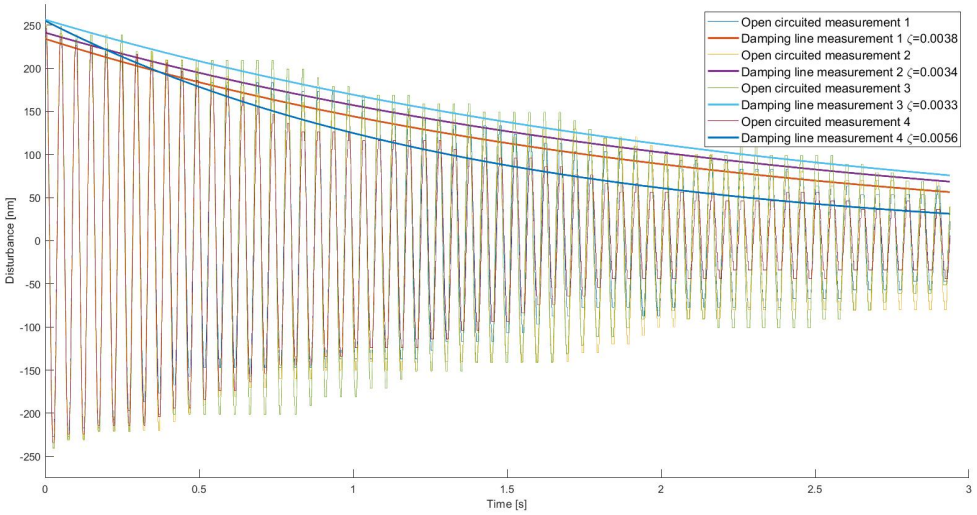

(a) This graph shows four measurements with the piezoelectric patches in open circuit at a starting amplitude of around 250 nm.

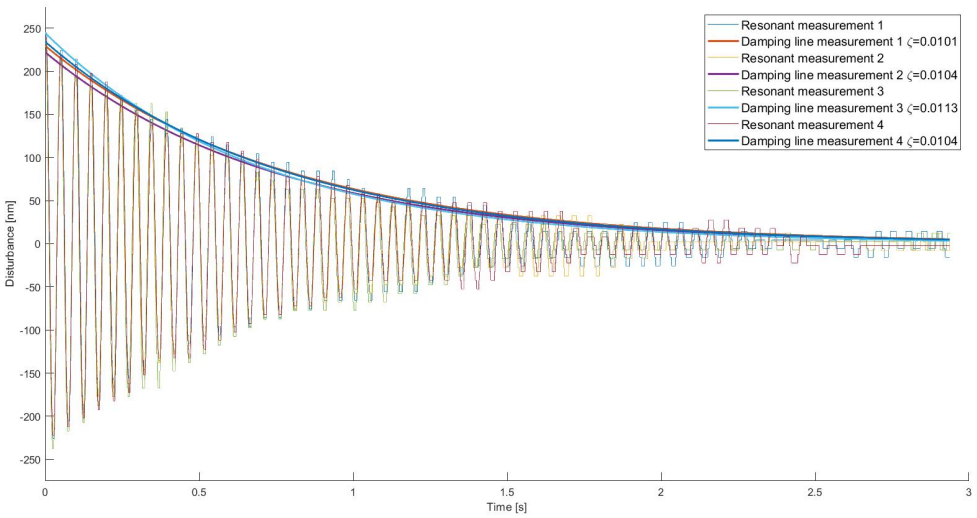

(b) This graph shows four measurements with the piezoelectric patches with a resonant shunt at a starting amplitude of around 250 nm.

Figure 5.5: Eight measurements at an amplitude of 250 nm, were in four measurements the piezoelectric patches are open circuited and in four measurements they have a resonant shunt.

To compare the measurements shown in 5.5b the mean and standard deviation of the four open circuited measurements and the resonant shunt measurements were calculated for every point in time. This ensures that the effect of the ground motion is reduced by $\sqrt{4}$. The means and the ±95% confidence interval of the peaks are then plotted and are shown in figure 5.6.

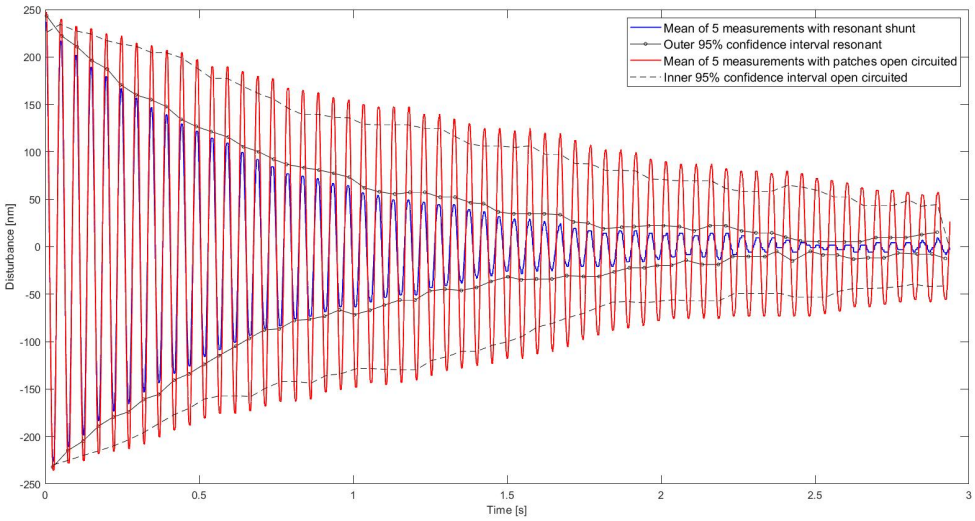

Figure 5.6: In this figure, the ten measurements, where four are open circuited and four have a resonant shunt, are shown. It shows the mean of the open circuited measurements, the mean of the resonant shunt and their respective 95% confidence interval.

This figure shows that the resonant shunt is damping the setup. The outer 95% confidence interval lines of the resonant shunt are well within the inner confidence interval lines of the open circuited situation. The next step is to determine the damping ratio. This is done by taking the absolute of the measurement and fitting the $Ae^{-\zeta\omega t}$ to the measurement. An example of this is shown in figure 5.7.

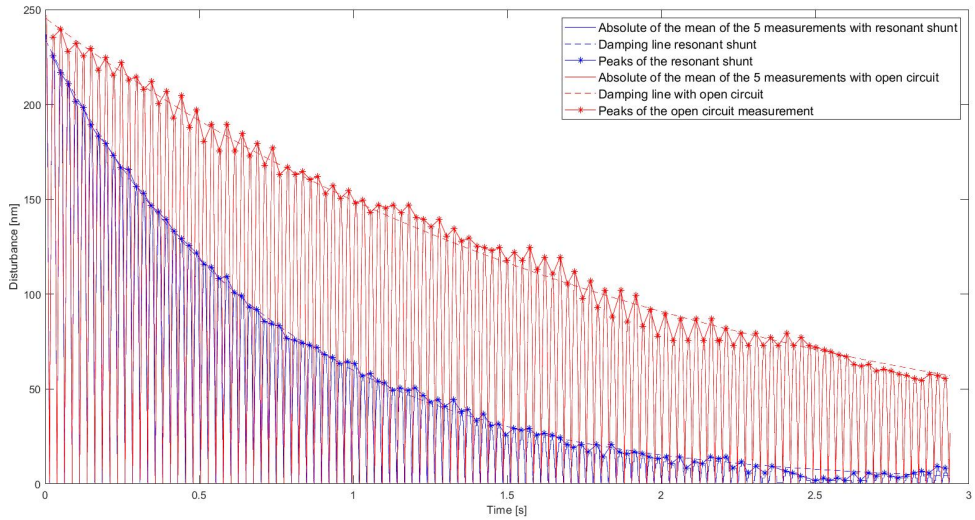

Figure 5.7: In this figure, the ten measurements, where four are open circuited and four have a resonant shunt, are shown. It shows the mean of the open circuited measurements, the mean of the resonant shunt and their respective 95% confidence interval.

This results in $\zeta = 0.004 \pm 8.1 * 10^{-5}$ with a 95% confidence interval for the fit for the open circuited situation. In the case of the resonant shunt, this equates to a $\zeta = 0.011 \pm 1.2 * 10^{-4}$. Again the 95% confidence interval for the damping ratio is for the fit.

5.2.3. Comparison at 100 Nanometres Amplitude

In this section, the resonant shunt is compared to the open circuited situation at 100 nm. The same results shown in figure 5.6 are shifted to 100 nm. The result of this shift is shown in figure 5.8.

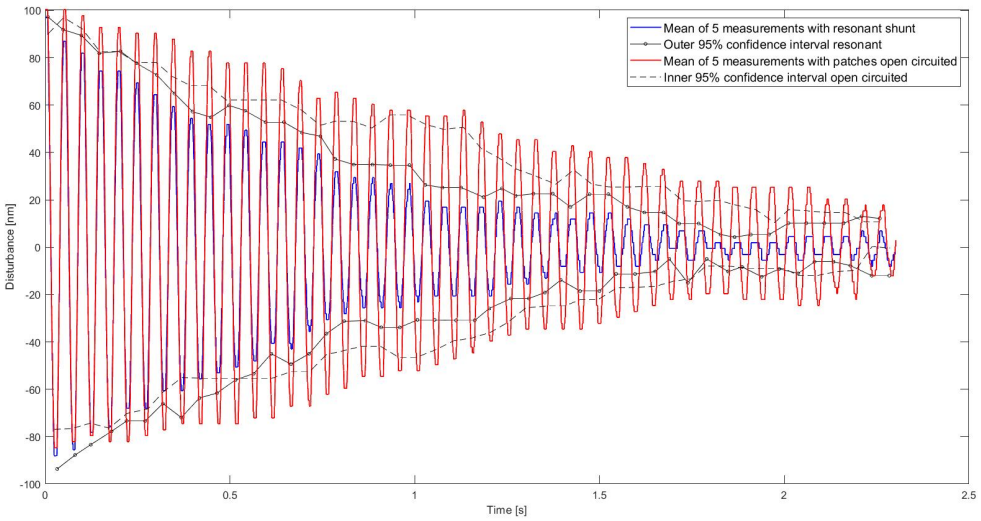

Figure 5.8: In this figure, the eight measurements, where four are open circuited and four have a resonant shunt, are shown at 100 nm. It shows the mean of the open circuited measurements, the mean of the resonant shunt and their respective 95% confidence interval.

In this figure, only the outer 95% confidence bounds of the resonant measurements are shown and the inner bounds of the open circuited situation. In this situation, since most of the outer confidence interval of the resonant shunt still remains within the inner confidence interval of the open circuited situation it is again judged to be damping. Again the damping ratio is calculated by taking the absolute of the measurements and fitting $Ae^{-\zeta\omega t}$ to the measurement. This results in a resonant damping ratio of $\zeta = 0.011 \pm 3.4 * 10^{-4}$ and for the open circuited situation: $\zeta = 0.0055 \pm 3.1 * 10^{-4}$. Thus, it can be concluded that the resonant shunt is damping at 100 nm as well.

5.2.4. Comparison at 50 Nanometres Amplitude

Again the data is shifted. This time until amplitude is reduced to 50 nm with only the outer 95% confidence bounds of the peaks of the resonant shunt and the inner 95% confidence bounds of the open circuited situation shown. The resulting graph is shown in figure 5.9.

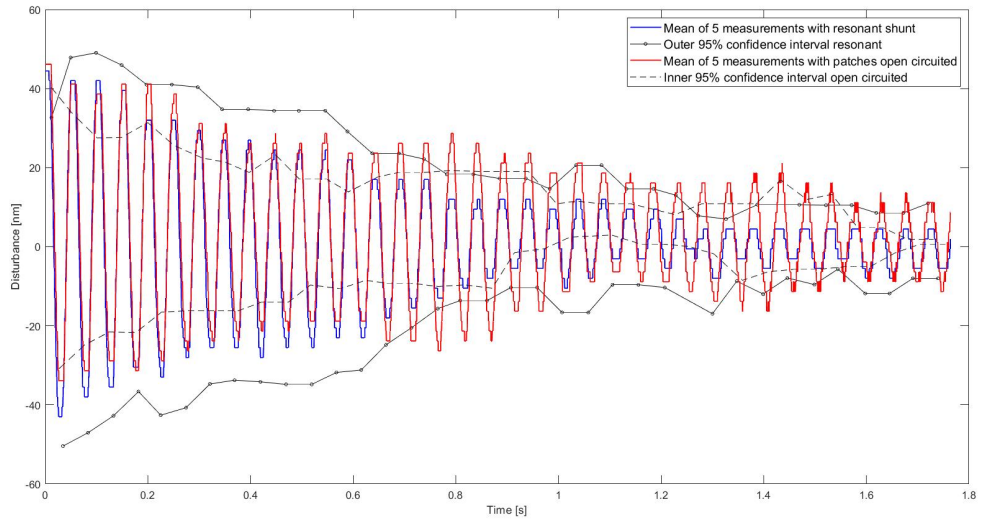

Figure 5.9: In this figure, the eight measurements, where four are open circuited and four have a resonant shunt, are shown at 50 nm. It shows the mean of the open circuited measurements, the mean of the resonant shunt and their respective 95% confidence interval.

The determined damping ratio for the resonant shunt is $\zeta = 0.012 \pm 8.1 * 10^{-4}$ and for the open circuited situation: $\zeta = 0.0053 \pm 8.1 * 10^{-4}$. Since the inner confidence interval lines of the open circuited situation are within the confidence interval lines of the resonant shunt, it is determined that we can not be sure that it is damping, however, it is a clear indication that it is still damping at 50 nm. Using the worst case scenario, though, it is decided that the lowest amplitude where damping is reached is in the 100 nm amplitude range.

6

Conclusion

The goal of this thesis is to answer the following main question: *how to attenuate remaining sub-nanometre amplitude vibrations with low frequency using piezoelectric shunt damping?* This question is further explored with three subquestions.

1. Does piezoelectric shunt damping work at this small amplitude and does damping even work at this small amplitude?
2. How does piezoelectric shunt damping work, what types of shunts are there and what are their advantages and disadvantages?
3. How to add piezoelectric damping to a vibration control system and how to deal with the stiffness of the piezoelectric transducer at this low resonance frequency?

Through the literature study and looking at the state of the art, it was found that piezoelectric transducers can actuate at sub-nanometre amplitude [17]. The use of piezoelectric shunt damping in nanopositioning by Eielsen et al. [4], shows that it works at nanometre level. Although, in this case the mode that was damped had a resonance frequency of 1.84 kHz. No clear research has been found that uses passive piezoelectric shunt damping with a low resonance frequency and at (sub)nanometre level amplitude. However, there is research that suggests the possibility of this application. Thus, too answer the first sub question fully, research needs to be done into piezoelectric shunt damping at (sub)nanometre amplitude and low resonance frequency.

The literature study shows the working principles of piezoelectric shunt damping and what types of shunts there are. Since only the resistive shunt and the resonant shunt are used, these are the only two which are shown in the thesis. Additionally it is explained how to deal with the high stiffness of the piezoelectric transducer and how to attain a low resonance frequency.

To determine if piezoelectric shunt damping works at (sub)nanometre level and with low resonance frequency, an experimental setup was built. This setup uses inverted pendulums to reduce the stiffness of the setup. However, the setup's resonance frequency was increased to 20 Hz, since the vibration isolation tables reduce the ground motion more are at this frequency compared to lower frequencies.

In order to determine if piezoelectric shunt damping is feasible at nanometre amplitude and low resonance frequency, a four-step plan was implemented, which is shown below.

1. Reduce ground motion in the setup so we are able to measure the damping at the lowest amplitude obtainable with the available hardware.
2. Use a simple resistive shunt and see at what amplitude it will damp.
3. Increase the sensor resolution to see if sub-nanometre amplitude damping can be achieved.
4. Try different shunts to see how much damping can be achieved.

The ground motion was reduced using vibration isolation tables. Although it could not reach the sub-nanometre amplitude in vibration reduction, it was reduced to 16.4 nm RMS. This is done by using an active vibration isolation table stacked upon a passive vibration isolation table. This means that sub-nanometre experiments are not feasible unless the ground motion is further reduced by other means.

However, nanometre experiments can be done. Which was why the next step was to use a resistive shunt to see until what amplitude it is damping. The obtained damping ratio for the resistive shunt at larger amplitude is 0.0036, which is not a lot, but still larger than the open circuited situation. Due to this small amount of added damping of the resistive shunt, at 250 nm the results are inconclusive. It was hypothesised that when larger damping is achieved by using a resonant shunt, a better and clearer distinction between damping can be found at these lower amplitudes.

It was shown that the resonant shunt was damping the system, with certainty, at 250 and 100 nm. The resonant shunt had a damping ratio of $\zeta = 0.011$ with a for the 250 nm measurements and for the 100 nm. However when the amplitude was reduced to 50 nm, the confidence intervals of the open circuited and resonant shunt were overlapping and thus the effect of the ground motion on the setup was too large to prove damping with certainty. Therefore, it can be concluded that piezoelectric shunt damping works at 100 nm amplitude and 20 Hz, but not at lower amplitudes. This partly answers the first sub research question, since this proves piezoelectric shunt damping at nanometre amplitude, but not at sub-nanometre amplitude.

7

Discussion and Recommendations

In this chapter some problems encountered during the thesis and research will be discussed. Some recommendations on how to avoid these problems and some recommendations which help conduct further research be given.

The first thing to discuss is the increase of resonance frequency of the experimental setup. The frequency was increased to accommodate the vibration isolation of the vibration isolation tables. Most of these commercially available tables only start to give a usable vibration reduction around 10 to 20 Hz. To get to these lower frequencies (such as 2 Hz) a custom vibration isolation platform might be needed to actually test the performance.

Another point of discussion is the ground motion. Since no seismometers were used to determine the ground motion in the lab, it is difficult to interpret the different peaks within the power spectral density and their causes. Having the seismometers would also help getting a clearer indication of the vibration isolation performance of the setup when they are used on the different vibration isolation stages. Another reason why the seismometers might be useful is that when they are placed next to the fine stage, on top of the vibration isolation stages, the actual ground motion could probably be used as an input and used to determine the damping ratio.

The decision to increase the length of the flexures is an important point for discussion. Due to the increase of the flexures and not only the thickness, it is surmised that the damping performance of the shunts are decreased, as is explained in Chapter 3.2.3. The original intention of increasing the length of the flexure was because in Kruik [16] it was observed that when the piezoelectric patches covered only 20% of the beam, the damping performance is very close to optimal. The mistake made however, is that piezoelectric shunt damping is likely more similar to the passive constrained layer damping presented in his thesis and not the active damping for which the 20% was determined. This means that increasing the patch length and placing patches at the top and the other side of the beam would likely have increased the damping performance. This is supported by Liao and Sodano [19], where a beam fully covered on both sides is tested. It appears that they achieve a loss factor of 0.055 and a damping ratio which is a slightly higher than 0.025. Which is a lot higher than the achieved damping ratio in this research. Thus, it is recommended to perform additional research (either literary or experimental) on the effect of patch size and its location and damping performance.

An additional benefit of reducing the length of the flexures, is that the unexpected second mode of the experimental setup is likely to be removed if the experimental setup is returned to its original beam length. Mainly because in its original state there is only one mode and there is no reason to suggest that by purely increasing the thickness of the beams and adding piezoelectric patches to the setup a second mode appears.

Not only reducing the flexures, and thus increasing the coverage of the piezoelectric patch, could increase the damping performance, but a better connection between flexure and beam is expected to be beneficial as well. In this research, only one iteration of glueing was tried and the actual glue layer might have been thicker than wanted. At least it is expected that the process could be optimised. For example, using a mold to keep

the piezoelectric patch in place might have helped with the positioning of the patches. Also, the glue put on the patch was probably excessive. The effect the glue and attachment has on the damping performance is unknown and should be researched further as well.

An additional point for discussion is the resonant shunt used in this research. It might not have reached its optimal damping performance since it is tuned to the two passive platform and not to the passive and active platform. The fact that the resistance was not varied either, but that the calculated resistor value (equation 2.5) was used, might also have a detrimental effect. In chapter 3.4, the noise in the resonant shunt due to the operational amplifiers and the resistors was also briefly discussed. In the experiment the resistive and resonant shunt appear to be damping, however, no research was done to actually discover the noise in both shunts and at what point the noise in shunt might have a detrimental effect on the damping. It appears that even with high noise resistors, damping can be achieved. This means that the working range of the synthetic inductor and the resistive shunt is likely to be lower than expected. Taking into account that the resonant shunt was not optimally tuned and that it did not have low noise components, the resonant shunt was more robust than expected. Thus it is expected that when further research is done into piezoelectric shunt damping at sub-nanometer amplitudes, the resonant shunt (when using low noise components) might function quite well. However, it is recommended to perform additional research on the vibration amplitude and noise within the resistive and resonant shunt.

A

Dynamics of the Passive Vibration Isolation Tables

In this appendix, the calculation for the two and three degree of freedom transmissibility is shown. In table **??**, the parameters used to calculate the transmissibility are shown. Note that most of these parameters are guesses. The damping calculated for the fine stage is assumed to be the same as the damping ratio found in Chen [2], which is about 0.0153. The stiffness of the *200BM-4* was determined by using the given minimum payload and the given resonance frequency of 0.5 Hz. The damping coefficient was determined from figure 3.2a and then verified by comparing the resulting graph to the graph in figure3.2a. The stiffness and damping coefficient for c_{BM2} and k_{BM2} are the same as c_{BM} and k_{BM}, in the case of the three degree of freedom transmissibility, the masses were changed though: $m_{BM} = 32\ kg$, which is the mass of the *200BM-4* vibration isolation table and $m_{BM2} = 50\ kg$.

Table A.1: The different parameters and their

Variable	m_{FS}	m_{BM}	k_{FS}	k_{BM}	c_{FS}	c_{BM}
Value	66 kg	0.57 kg	$9.5*10^3\ N/m$	650 N/m	16.6 Ns/m	0.58 Ns/m

A.1. Two degrees of freedom

To determine the dynamics, first equations A.1 are set up. The M, K, C and F matrices will differ depending on the two or three degree situation.

$$M\ddot{x} + Kx + C\dot{x} = F \tag{A.1}$$

$$F_1 = k_{BM}x_0 + c_{BM}\dot{x_0} \Rightarrow \frac{F_1}{X_0} = c_{BM}s + k_{BM} \tag{A.2}$$

In the case of the two degrees of freedom situation, the M, K, C, and F matrices are shown in equation A.3.

$$M = \begin{bmatrix} m_{BM} & 0 & 0 \\ 0 & 0 & m_{FS} \end{bmatrix} \tag{A.3}$$

$$K = \begin{bmatrix} k_{BM} + k_{FS} & -k_{FS} \\ -k_{FS} & k_{FS} \end{bmatrix}$$

$$C = \begin{bmatrix} c_{BM} + c_{FS} & -c_{FS} \\ -c_{FS} & c_{FS} \end{bmatrix}$$

$$F = \begin{bmatrix} F_1 \\ 0 \end{bmatrix}$$

Now by changing this formulation to the state space representation shown in equation A.4, the resulting A,B,C and D matrices for the two degrees of freedom situation are shown in equation A.6.

$$\dot{x} = Ax + Bu \tag{A.4}$$
$$y = Cx + Du \tag{A.5}$$

$$\dot{x} = \begin{bmatrix} \dot{x_{BM}} \\ \dot{x_{FS}} \\ \ddot{x_{BM}} \\ \ddot{x_{FS}} \end{bmatrix} = \begin{bmatrix} 0 & 0 & 1 & 0 \\ 0 & 0 & 0 & 1 \\ -\frac{k_{BM}+k_{FS}}{m_{BM}} & \frac{k_{FS}}{m_{BM}} & -\frac{c_{BM}+c_{FS}}{m_{BM}} & \frac{c_{FS}}{m_{BM}} \\ \frac{k_{FS}}{m_{FS}} & -\frac{k_{FS}}{m_{FS}} & \frac{c_{FS}}{m_{FS}} & -\frac{c_{FS}}{m_{BM2}} \end{bmatrix} \begin{bmatrix} x_{BM} \\ x_{FS} \\ \dot{x_{BM}} \\ \dot{x_{FS}} \end{bmatrix} + \begin{bmatrix} 0 \\ 0 \\ \frac{1}{m_{BM}} \\ 0 \end{bmatrix} \begin{bmatrix} F_1 \end{bmatrix} \tag{A.6}$$

$$\text{y} = \begin{bmatrix} 0 & 1 & 0 & 0 \end{bmatrix} \begin{bmatrix} x_{BM} \\ x_{FS} \\ \dot{x_{BM}} \\ \dot{x_{FS}} \end{bmatrix} + 0 \begin{bmatrix} F_1 \end{bmatrix}$$

Now, by using the *matlab* function *ss2tf*, the transfer function of $\frac{X_{FS}(s)}{F_1}$ can be found. To get the transfer function from the ground motion to X_{FS}, equation A.7 can be used. This transfer function results from equation A.1

$$\frac{F_1}{X_0} = c_{BM}s + k_{BM} \tag{A.7}$$

Then by multiplying both transfer functions, the transmissibility from ground motion to the fine stage can be calculated.

A.2. Three degrees of freedom

The same process described above is used for the three degrees of freedom situation. For the M,K,C and F matrices see equation A.8.

$$M = \begin{bmatrix} m_{BM} & 0 & 0 \\ 0 & m_{BM2} & 0 \\ 0 & 0 & m_{FS} \end{bmatrix} \tag{A.8}$$
$$K = \begin{bmatrix} k_{BM} + k_{BM2} & -k_{BM2} & 0 \\ -k_{BM2} & k_{BM2} + k_{FS} & -k_{FS} \\ 0 & -k_{FS} & k_{FS} \end{bmatrix}$$
$$C = \begin{bmatrix} c_{BM} + c_{BM2} & -c_{BM2} & 0 \\ -c_{BM2} & c_{BM2} + c_{FS} & -c_{FS} \\ 0 & -c_{FS} & c_{FS} \end{bmatrix}$$
$$F = \begin{bmatrix} F_1 \\ 0 \\ 0 \end{bmatrix}$$

The resulting A,B,C,D matrices are shown in equation A.9

$$\dot{x} = \begin{bmatrix} \dot{x_{BM}} \\ \dot{x_{BM2}} \\ \dot{x_{FS}} \\ \ddot{x_{BM}} \\ \ddot{x_{BM2}} \\ \ddot{x_{FS}} \end{bmatrix} = \begin{bmatrix} 0 & 0 & 0 & 1 & 0 & 0 \\ 0 & 0 & 0 & 0 & 1 & 0 \\ 0 & 0 & 0 & 0 & 0 & 1 \\ -\frac{k_{BM}+k_{BM2}}{m_{BM}} & \frac{k_{BM2}}{m_{BM}} & 0 & -\frac{c_{BM}+c_{BM2}}{m_{BM}} & \frac{c_{BM2}}{m_{BM}} & 0 \\ \frac{k_{BM2}}{m_{BM2}} & -\frac{k_{BM2}+k_{FS}}{m_{BM2}} & \frac{k_{FS}}{m_{BM2}} & \frac{c_{BM2}}{m_{BM2}} & -\frac{c_{BM2}+c_{FS}}{m_{BM2}} & \frac{c_{FS}}{m_{BM2}} \\ 0 & \frac{k_{FS}}{m_{FS}} & -\frac{k_{FS}}{m_{FS}} & 0 & \frac{c_{FS}}{m_{FS}} & -\frac{c_{FS}}{m_{FS}} \end{bmatrix} \begin{bmatrix} x_{BM} \\ x_{BM2} \\ x_{FS} \\ \dot{x_{BM}} \\ \dot{x_{BM2}} \\ \dot{x_{FS}} \end{bmatrix} + \begin{bmatrix} 0 \\ 0 \\ 0 \\ \frac{1}{m_{BM}} \\ 0 \\ 0 \end{bmatrix} \begin{bmatrix} F_1 \end{bmatrix} \quad \text{(A.9)}$$

$$x_{FS} = \begin{bmatrix} 0 & 0 & 1 & 0 & 0 & 0 \end{bmatrix} \begin{bmatrix} x_{BM} \\ x_{BM2} \\ x_{FS} \\ \dot{x_{BM}} \\ \dot{x_{BM2}} \\ \dot{x_{FS}} \end{bmatrix} + 0 \begin{bmatrix} F_1 \end{bmatrix}$$

Again to get the transfer function *ss2tf* is used and this resulting transfer function is then multiplied with the transfer function in equation A.7.

B

Accurion Halcyonics i4 Datasheet

solutions for science

Operating Instructions

_active vibration isolation desktop unit halcyonics_i4 series

Contents

1. Introduction

Thank you for purchasing the halcyonics_i4 system. By selecting this device you have acquired a top-of-the-line active vibration isolation equipment. We feel confident that our system will meet your expectations and provide the best possible performance for your specific application.

Please read the operating instructions carefully to set up the i4 system correctly.

We hope you enjoy working with your halcyonics_i4!

2. Unpacking the i4 System

After unpacking the system, please check whether the package contains all components.

Equipment supplied for the halcyonics_i4 system:

- 1 halcyonics_i4 system
- 1 power cord
- 1 power supply
- 1 instruction manual

3. Symbols used in these instructions

 Warning symbol

 Important note

 Action that the user is required to take

4. Safety Instructions and Warnings

Please read through the following safety instructions and warnings carefully before using this equipment.

General Warnings

Do not operate the system in a potentially explosive or humid environment. Do not switch on the system if there is any visible damage or if you think it might be damaged. In this case, turn off the power immediately and notify our distributor in your area or contact Accurion's headquarters in Germany directly.

Electrical Safety

This system may be operated only on AC grounded power. Do not interrupt the protective grounding conductor under any circumstances. If you plan to use a power cable other than the standard power cord supplied with this equipment, first check that the protective grounding conductor is connected.

Before starting to operate this equipment, check the voltage rating to be sure that it matches your local voltage. For further information, please refer to the specifications on page 10.

Only the certified, external power supply supplied with the system must be used.

Finish the set up and installation before attempting to plug it into an electrical outlet. Never open the equipment housing. Only authorized and qualified personnel may service or repair the equipment. The device must be connected to an easily accessible supply socket so that in the event of a malfunction, the supply plug can be removed quickly.

Mechanical Safety

Ensure that the equipment rests on a stable surface that can safely support the weight of this instrument.

Please note that you need to activate the transport/relocation locking mode before you transport or move the equipment! For further instructions, please refer to the section "Automatic Load Adjustment and Transport Locking Mode" on page 6.

Intended Use

The system is suited to isolate various measurement equipment from building vibration and other disturbing influences. Any other use is not permitted.

Never use the isolation system in mobile environments or outside the specified environmental and operational requirements, see page 10.

DIN and European Standards, European Council Directives

Halcyonics i4 systems conform to the requirements currently valid for electrical safety according to EC Directive 2014/35/EU and for electromagnetic compatibility according to EC Directive 2014/30/EU. This equipment has been tested and found to comply with the following standards EN 61010-1:2010.

5. Getting Started and Operation

Setting Up the System

To obtain best performance from the halcyonics_i4, set it up on a stable, rigid and flat surface. For optimal operating results, the planarity of the support surface should be 0.5 mm.

If you set up the i4 system on a table or bench frame, make sure that the table is distortion-free and stiff. Although most tables and bench frames have sufficient resistance to vertical vibration, they are relatively sensitive with respect to horizontal vibration. This causes amplification of structure and airborne noise.

Therefore, to set up your vibration isolation equipment, select a place with a vibration level that is as low as possible. Vibration generated at this place should not exceed velocities of 500 µm/s.

Operating the system at low temperatures may cause malfunctioning. If the equipment is brought from a cold environment into a relatively warmer one, we recommend that you wait approx. 2 – 3 hours before plugging it into AC power and switching on the power.

Start-up

- Set up the system on a flat, stable surface at your work area.
- Connect the external power supply to AC power (main supply) and to the i4.
- Center your application on the top plate of the i4 system.
- Turn on the power switch on the front panel of the system.
- Press the Load Adjust button for automatic load adjustment (see page 6)
- Set the switch for active isolation to on, blue LED is on (see page 7)

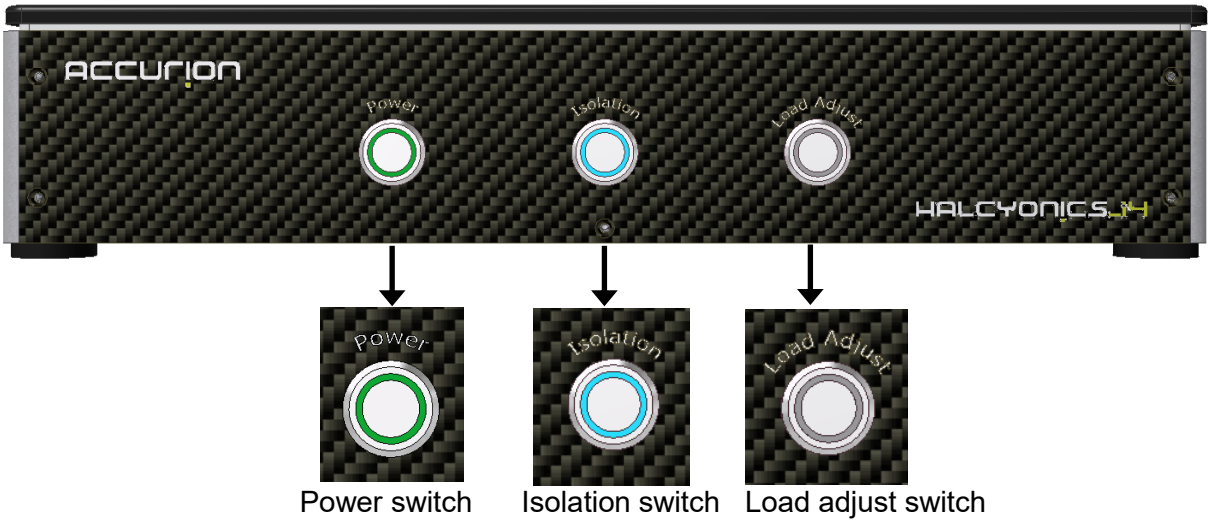

Power switch Isolation switch Load adjust switch

Automatic Load Adjustment and Transport Locking Mode

The top plate of the system is supported by four steel springs. These springs carry the load placed on top. For the initial installation or after load changes these springs have to be pre-stressed according to the weight of the setup. This is done by electric motors via an electronic circuit. This procedure is called „automatic load adjustment“. The objective of the load adjustment is to elastically support the top plate by the springs.

The halcyonics_i4 systems have a combined automatic load adjustment and transport locking mode feature. Both functions are controlled using the "Load Adjust" button The following modes can be selected depending on the number of times you press the button. The LEDs show the selected mode as follows:

- Green – load adjustment
- LED off – neutral
- Red – transport locking mode

The "load adjustment" mode (green LED) is used for automatic, load-dependent adjustment of the system. When you set up the system and press this button, the system will start the load adjustment. For initial adjustment and for changing the loading conditions, the green mode has to be selected. During the activation of the green LED, the system will check at intervals whether the load on the system has changed and will automatically move the top plate into the optimal position when necessary. If this automatic adjustment is not desired, please turn the LA-Automatic off by pressing the load adjust button once so that the LED is off. During the load adjustment of the i4 system, the active isolation is interrupted.

The “neutral” mode (LED off) is selected to deactivate the automatic load adjustment and to avoid the self-adjustment of the system. This way the motors of the load adjustment do not start to run at an unwanted time. Once you switch on the system power for the first time, the i4 system will be in the "neutral" mode. At this point, select the "load adjustment" mode. As soon as the stepper motors stop you can switch to "neutral" and the system is ready to operate.

Press and hold the button for 4 seconds!

During transportation the halcyonics_i4 system always has to be locked! In the lock mode a rigid mechanical contact between the top and the bottom of the system prevents the sensitive components from damage. To lock the system, change the load adjustment setting to the "transport locking mode" (red LED), and the four steel springs will be automatically pre-stressed up to the maximum.

The system may only be transported or moved in the transport-locked condition!

There must not be any load on top of the isolation system during transport!

To change the different modes, it is necessary to press and hold the button for some seconds.

Using Active Vibration Isolation

Once you have started up the system, press the “isolation” button on the front panel to enable the active vibration isolation. Now the system initializes, which is shown by a flashing blue LED. When the system initializes for the first time or after a long interval, this process can take up to 30 seconds. When the blue LED remains lit, the active vibration isolation is activated.

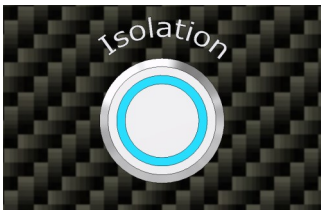

Overmodulation of the System

The i4 has been designed to compensate vibration amplitudes up to 500 µm/s. If vibrations significantly exceed this level the system changes to the stand-by mode, indicated by a flashing blue "Isolation" LED. After the overload excitation is stopped, the isolation mode will automatically be turned on again. After a severe overload the system may take up to 30 seconds to reach full active isolation performance, but normally only a few seconds are required.

The active vibration isolation will be automatically switched off during overmodulation of the system. Once this interference has subsided, the system will re-initialize and, after a few seconds, automatically resume to the active isolation mode. This procedure does not require any action from the user.

6. Appendix

Care and Maintenance

The i4 system has been carefully designed and manufactured by Accurion. To maintain this equipment and the validity of your warranty, you should observe the following recommendations:

- Store the system in a dry place. Never expose it to rain, liquids or dampness. The minerals contained in these liquids may lead to short-circuits or corrosion of the electronic circuits.
- Where possible, avoid operating and storing the system in dirty or dusty environments as this may otherwise damage the electronic or mechanical components.
- Do not store the system in hot environments. Operating the system at high temperatures may compromise its performance and reduce its lifetime.
- Do not store the system in cold environments. When the temperature rises to normal room temperature, moisture condenses inside the system and causes a circuit failure. If you need to transport the system from a cold environment to a warmer one, wait approx. 2 – 3 hours before plugging it into AC power and switching on the power.
- Do not drop the system or shake it, and never expose it to impact or blows. Improper handling can damage the integrated electronics and mechanical components in the system.
- To clean, wipe off dust from the exterior surfaces of the system using a lint-free cloth. For cleaning, do not use any aggressive cleaning agents.

EMC Test Report

Test schedule and results – EMC - Immunity and Emission

DAkkS Deutsche Akkreditierungsstelle D-PL-12047-01-01 D-PL-12047-01-03 D-PL-12047-01-04

Accredited EMC-Test Laboratory

CETECOM™

Type of device		**Active Vibration Isolation Desktop Unit**
Type name		**halcyonics i4 series**
Serial number		**i4 – TI – 5928**
Variant type name		**i4medium, i4large, workstation i4**
Manufacturer		**Accurion GmbH** **Stresemannstr. 30, 37079 Göttingen (Germany)**
Applicant		**Accurion GmbH** **Stresemannstr. 30, 37079 Göttingen (Germany)**
Test Standards	**Immunity:**	**EN 61326-1:2013** **include tests according to :** EN 61000-4-2:2009 EN 61000-4-3:2006 + A1:2008 + A2:2010 EN 61000-4-4:2012 EN 61000-4-5:2006 EN 61000-4-6:2009 EN 61000-4-11:2004
	Emission :	**EN 55011:2009 + A1:2010** **EN 61000-3-2:2014** **EN 61000-3-3:2013**
Configuration and operation mode		See Test reports
Performance Criteria (Immunity)		General criteria according to EN 61326-1

Performance criterion A

The equipment shall continue to operate as intended during and after the test. No degradation of performance or loss of function is allowed below a performance level specified by the manufacturer, when the equipment is used as intended. The performance level may be replaced by a permissible loss of performance. If the minimum performance level or the permissible performance loss is not specified by the manufacturer, either of these may be derived from the product description and documentation and what the user may reasonably expect from the equipment if used as intended.

Performance criterion B

The equipment shall continue to operate as intended after the test. No degradation of performance or loss of function is allowed below a performance level specified by the manufacturer, when the equipment is used as intended. The performance level may be replaced by a permissible loss of performance. During the test, degradation of performance is however allowed. No change of actual operating state or stored data is allowed. If the minimum performance level or the permissible performance loss is not specified by the manufacturer, either of these may be derived from the product description and documentation and what the user may reasonably expect from the equipment if used as intended.

Performance criterion C

Temporary loss of function is allowed, provided the function is self-recoverable or can be restored by the operation of the controls.

CETECOM GmbH
Mundelheimer Weg 35
40472 Düsseldorf
Tel.: +49 (0) 211 - 171 497-0
Fax: +49 (0) 211 - 171 497-27

Specifications

Available Standard Versions		
halcyonics_i4	halcyonics_i4medium	halcyonics_i4large
halcyonics_i4 M6/25	halcyonics_i4medium M6/25	halcyonics_i4large M6/25
	halcyonics_i4medium 150 kg	halcyonics_i4large 150 kg
	halcyonics_i4medium 150 kg M6/25	Halcyonics_i4large 150 kg M6/25
Performance Specifications		
Isolation Technology:	Accurion control technology based on piezoelectric type acceleration pickup, fast signal processing and electro-dynamic type force transducers	
Force directions:	Active compensation in all six degrees of freedom	
Isolation performance:	> 5 Hz = 25 dB (94.4%); >10 Hz = 40 dB (99.0%)	
Active bandwidth:	0.6 – 200 Hz*	
Settling time:	300 ms**	
Response time:	0.5 ms***	
Max. correction forces:	Vertical ± 8 N; horizontal ± 4 N	
Load capacity:	i4: 0 – 120 kg (0 - 265 lbs) / i4medium + i4 large: 0 - 105 kg (231 lbs) or 40 - 150 kg (88 - 330 lbs)	
Other Specifications		
Dimensions:	i4: 400 x 500 x 90 mm (15.7“ x 19.7“ x 3.5“) / i4medium: 600 x 600 x 90 mm (23.6“ x 23.6“ x 3.5“) / i4large: 550 x 700 x 92 mm (21.7“ x 27.6“ x 3.6“)	
Weight:	i4: 20 kg (44 lbs) / i4medium: 37 kg (81 lbs) / i4large: 40 kg (88 lbs)	
Table top material:	Powder coated aluminium	
Top plate surface flatness:	± 0.10 mm over complete surface	
Max. compensation level:	500 µm/s at 6 Hz and with a load of 60 kg (132 lbs)**	
Repeatability of load adjustment:	120 µm	
Environmental and Operational Requirements		
Electrical voltage:	100 - 240 V AC/47 – 63 Hz	
Fuse (inside i4):	250V / F3,15A (Fuse may be changed by authorized service staff only!)	
Power consumption:	Typically 40 - 45 W	
Operating temperature:	15 – 40°C (59 – 104 F)	
Operating humidity:	0 – 60%	
Operating altitude:	< 2500 m (8100 ft)	
Operating condition:	Use in non-mobile laboratories only	
Pollution degree:	2 (according to DIN EN 61010-1)	

* Floating table top is supported by steel springs; low-pass characteristics of spring-mass combination dominates the dynamic behaviour above 200 Hz.

** The settling time and maximum compensation level depend on several conditions, such as payload, frequency, load distribution and height of the payload. For that reason this value should be considered as an estimation.

*** The response time determines when the system starts to actively isolate an incoming vibration after detection by the sensors.

Dimensions of the Isolator

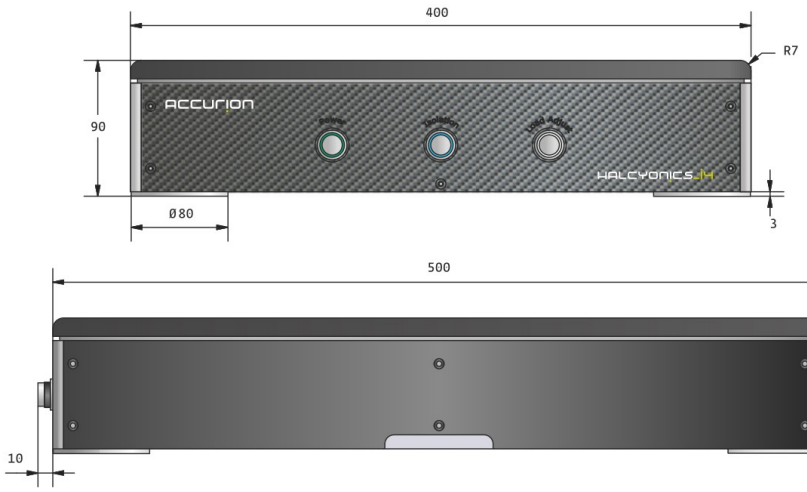

i4 system

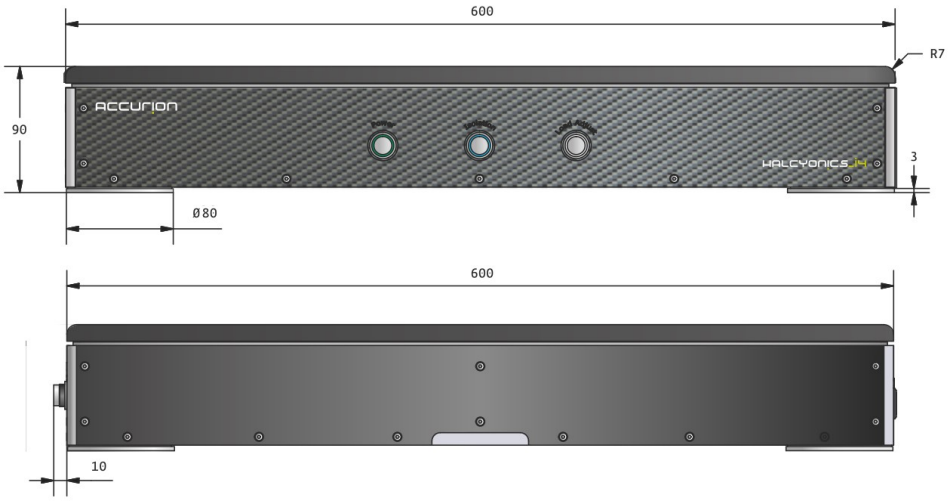

i4medium system

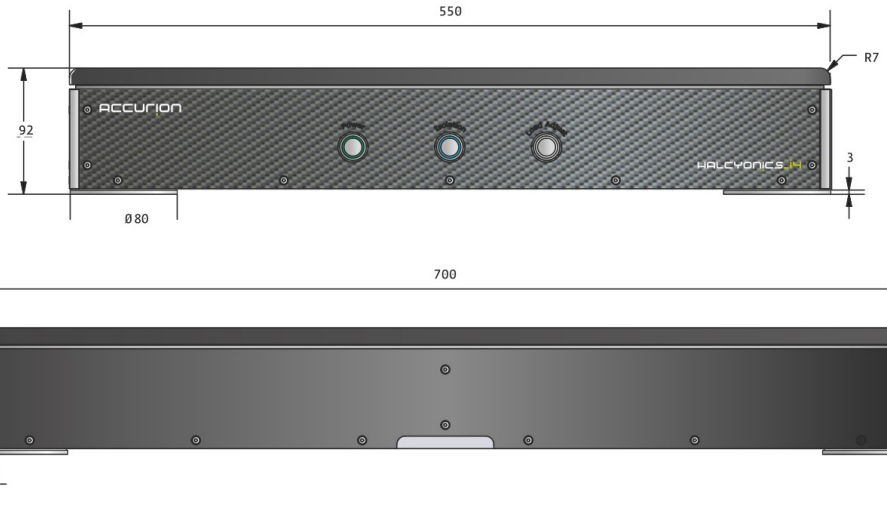

i4large system

Transmissibility

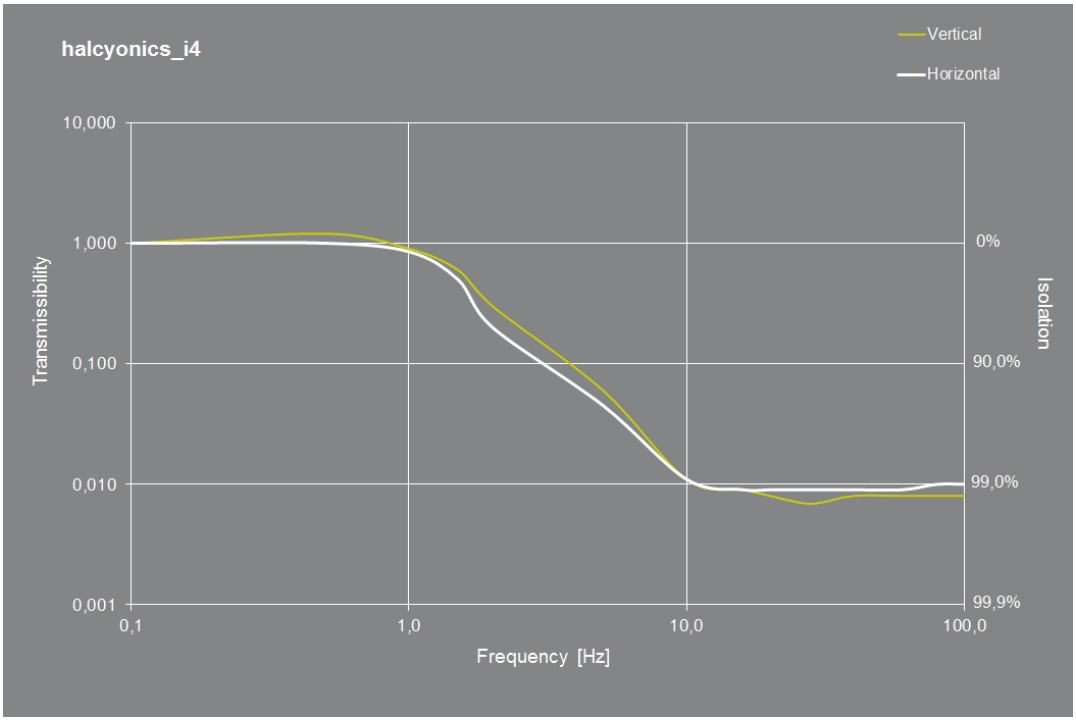

Transmission graph i4, measured at a velocity of 100 µm/s with a payload of 20 kg (44 lbs)

Settling Time

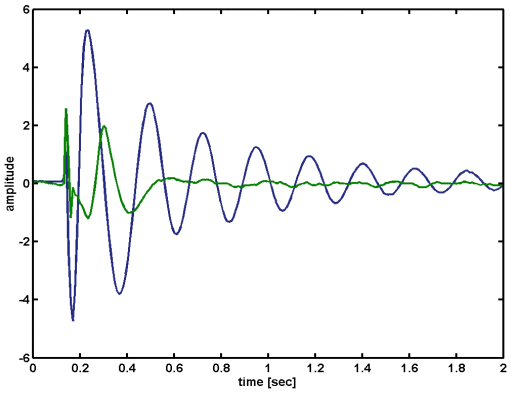

Settling time of a Halcyonics_i4 system (green) compared to a conventional air-damped vibration isolation system (blue), made by one of the major manufacturers of optical tables and vibration isolated laboratory desks.

Dynamic Stiffness

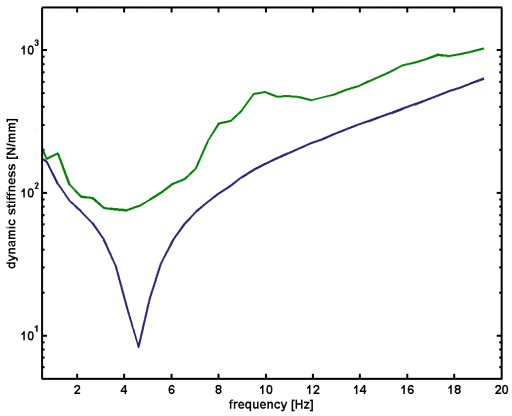

Dynamic isolator stiffness (green) of Accurion's i4 system compared to a commercially available passive air-damped isolation system (blue). Due to their higher dynamic stiffness, Accurion's systems are less sensitive to direct forces affecting the isolation system.

Accurion Offices

Headquarters Germany

Accurion GmbH
Stresemannstrasse 30
37079 Goettingen
Germany

Phone: +49-[0]551-99960-0
Fax: +49-[0]551-99960-10
E-Mail: info@accurion.com
www.accurion.com

North America

Accurion Inc.
20045 Stevens Creek Blvd., Suite 2E
Cupertino, CA 95014
USA

Phone/Fax: (+1) 408 642 1446
E-Mail: info@accurion.com
www.accurion.com

India

Accurion Scientific Instruments Pvt., Ltd.
Flat 402, Wing 2, Balaji Lakeside Marvel
#1413/2A, 7th Cross, 1st Main Road
BHCS Layout, Uttarahalli
Bangalore 560061
India

Phone: +91-[0]98450 04273
E-Mail: sharma@accurion.com
www.accurion.com

China

Accurion Scientific Instruments (Shanghai) Co., Ltd.
Rm. 502, Xuhui Commercial Building
No. 168, Yude Road, Xuhui District
Shanghai 200030
China

Phone/Fax: +86-[0]21-5017-9099
Mobile: +86-[0]138-1861-2900
E-Mail: FZ@accurion.cn
www.accurion.com.cn

Installation Video

C

Minusk 200BM-4 Datasheet

BM-4 Bench Top Vibration Isolation Platform

Weight: Approximately 60 lb (27 kg)

Dimensions: 16.8" W x 16.8" D x 8.5" H
(427mm W x 427mm D x 216mm H)

Approximate payload weight range:

Model	Payload Range
25BM-4	0 - 25 lb (0 - 11 kg)
50BM-4	20 - 55 lb (9 - 25 kg)
100BM-4	50 - 105 lb (23 - 48 kg)
150BM-4	90 - 155 lb (41 - 70 kg)
200BM-4	145 - 205 lb (63 - 93 kg)

Performance

- Vertical natural frequency of 1/2 Hz or less can be achieved over the entire load range.
- Horizontal natural frequency is load dependent. 1/2 Hz or less can be achieved at or near the upper limits of the payload range.

Simple Set-Up and Adjustment

The most cost effective bench top platform capable of 1/2 Hz performance vertical and horizontal.

For more information contact us at: 310-348-9656 or sales@minusk.com

The curve below shows the typical vertical 1/2 Hz performance of the BM-4. It offers 10-100 times better performance than typical high-performance air tables.

Typical Performance Curve:

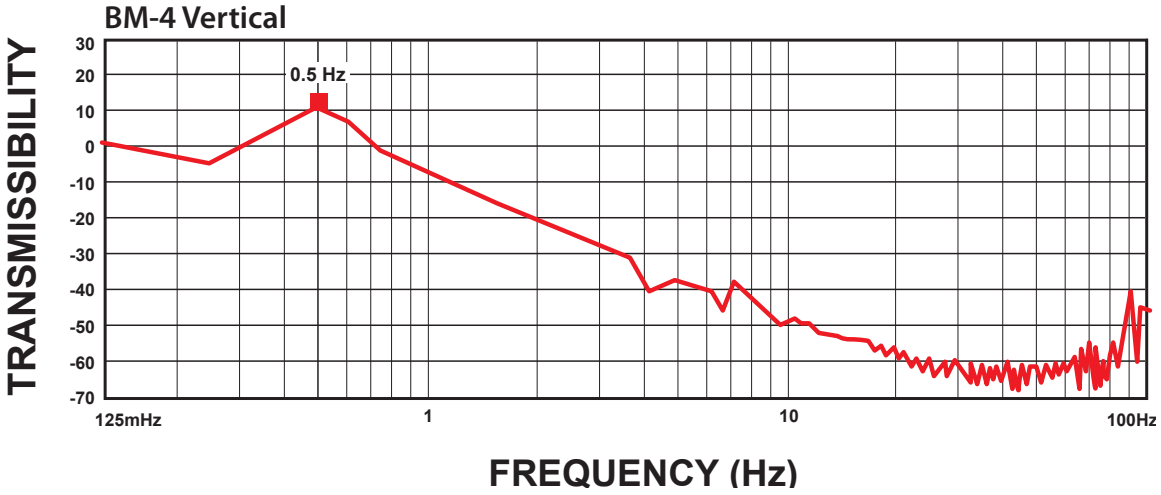

3/12

460 Hindry Ave., Unit C, Inglewood, CA 90301
www.minusk.com sales@minusk.com
Tel: 310-348-9656 Fax: 310-348-9638

minus k® TECHNOLOGY

Installation and Adjustment

BM-4 Bench Top
Vibration Isolation Platform

Dimensions: 16.8” W x 16.8” D x 8.5” H (427mm W x 427mm D x 216mm H)	
Approximate payload weight range:	
Model	Payload Range
25BM-4	0 - 25 lb (0 - 11 kg)
50BM-4	20 - 55 lb (9 - 25 kg)
Weight: Approximately 70 lb. (32 kg)/(same dimensions)	
100BM-4	50 - 105 lb (23 - 48 kg)
150BM-4	90 - 155 lb (41 - 70 kg)
200BM-4	145 - 205 lb (66 - 93 kg)

460 Hindry Ave., Unit C, Inglewood, CA 90301
Tel: 310-348-9656 Fax: 310-348-9638
www.minusk.com sales@minusk.com

minus k® TECHNOLOGY

BM-4 Bench Top
Vibration Isolation Platform

Installation and Adjustment

Required tools:

3/16 hex key
5/16 hex key
1/2 inch open-end wrench

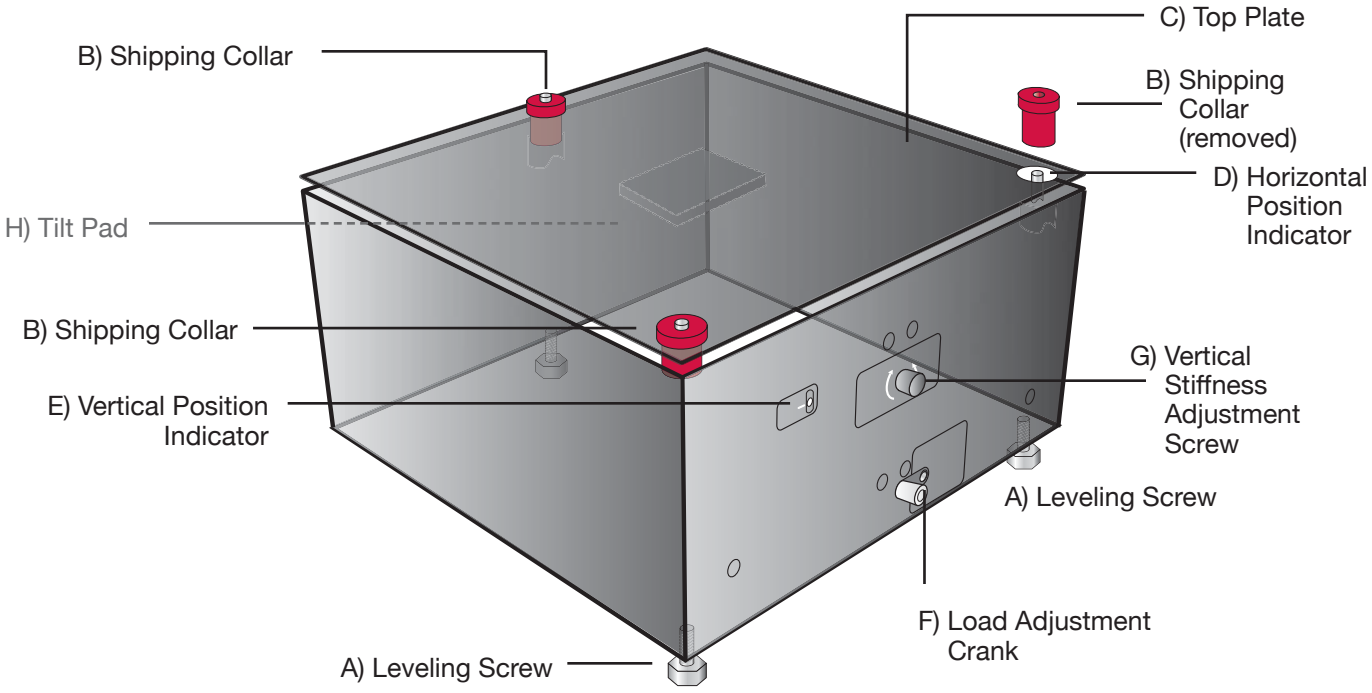

DO NOT REMOVE SHIPPING COLLARS UNTIL INSTRUCTIONS INDICATE. SHIPPING COLLARS MUST BE USED WHEN MOVING ISOLATOR.

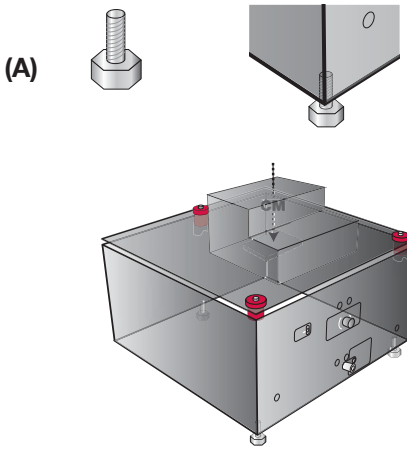

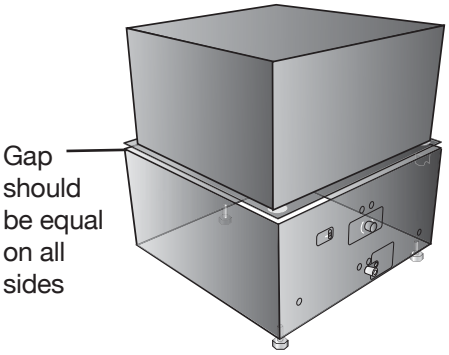

1. Make sure you have the correct model for your payload. Payload weight MUST be within the recommended range.

2. Locate the three (3) leveling screws (A). Insert the leveling screws into the bottom of the isolator and place on a solid, level surface. Place the bubble level on the top plate and use the leveling screws to level the isolator.

3. Carefully position payload on top plate so its center-of-mass (CM) is as close to center as possible.

4. Remove the three (3) red shipping collars (B). STORE SHIPPING COLLARS IN A SAFE PLACE AS THEY MUST BE USED WHENEVER MOVING ISOLATOR. Replace the screws into the holes to serve as Horizontal Position Indicators.

CAUTION: If payload covers shipping collar holes, collars must be removed before placing payload. Take extra care when placing payload without shipping collars attached. Do not replace screws as they may interfere with payload.

5. Check the level of the top plate. The gap between the top plate and the isolator cover should be approximately equal on all sides.

6. Reposition the payload, as necessary, to level the top plate. It is recommended that you re-install the red shipping collars if you need to re-position the payload (see Step 3). However, it is not necessary if you take extra care repositioning the payload. Do not use leveling screws to level the top plate.

NOTE: Cables, hoses, etc. connected to the payload can affect the horizontal and vertical position. If possible make the following adjustments without attaching the cables.

Floating Isolator Vertically

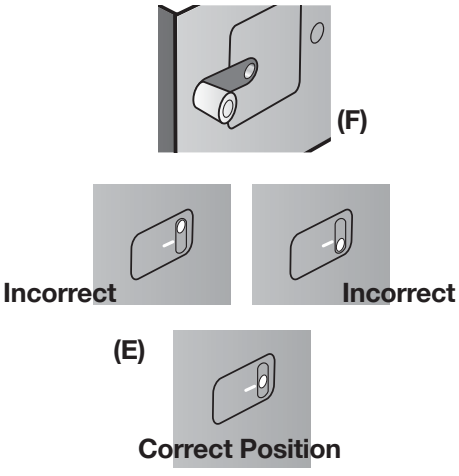

The isolator comes from the factory adjusted to support the nominal weight, i.e., 25 lb for the 25BM-4, 50 lb for the 50BM-4, etc. Internal stops limit vertical motion. The isolator must be “floated” between the stops.

7. Check Vertical Position Indicator (E). The pin should be approximately centered on the horizon line. Turn Load Adjustment Crank (F) only clockwise when the pin is below the line, and only counterclockwise when it is above the line. If the payload weight varies from nominal weight by a few pounds/ kilograms it may take many turns (approximately 10 turns per payload pound, 22 per kilogram).

NOTE: To avoid damage never force the Load-Adjustment Crank. If pin cannot be easily centered on line, turn Vertical Stiffness Adjustment Screw slightly counterclockwise and readjust vertical position. Repeat as necessary. This is a very sensitive adjustment. Turn the screw only a few degrees each time.

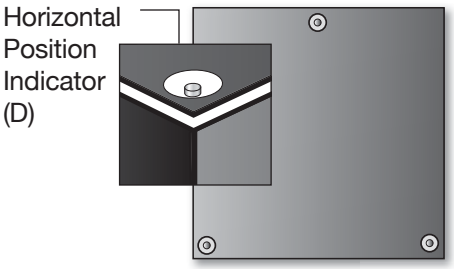

Top View

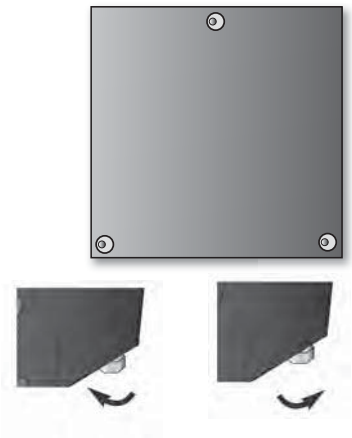

1/2 Hz = 3 cycles in 6 secs.

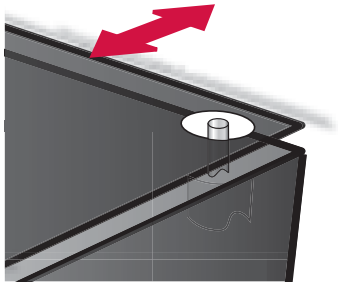

1/2 Hz = 3 cycles in 6 secs.

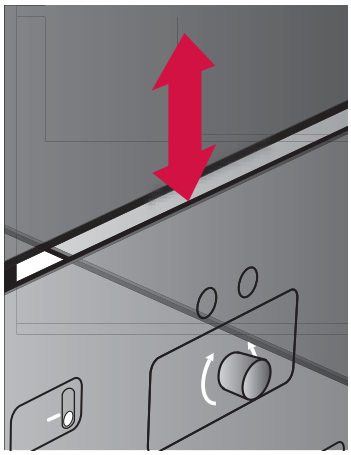

Floating Isolator Horizontally

8. Internal stops limit the horizontal motion. The isolator must be “floated” horizontally between the stops by adjusting the leveling screws. Horizontal Position Indicator screws (D) should be approximately centered within holes.

Example: If screws are too far to the left of center, turn front left leveling screw counterclockwise (as viewed from above) and front right leveling screw clockwise the same amount.

9. IF HORIZONTAL POSITION INDICATOR SCREWS ARE NOT VISIBLE, check positioning by pushing the top plate gently front to back then side to side. If it does not oscillate freely and independently front to back and side to side then adjust accordingly.

HORIZONTAL NATURAL FREQUENCY

10. The horizontal natural frequency can only be changed by varying the payload weight. 1/2 Hz is achieved when payload weight is near nominal (ie. 25 lb. for the 25BM-4). Increasing the weight lowers the frequency. Decreasing the weight raises the frequency. Ballast weights can be used for fine adjustments to frequency.

Check the horizontal frequency by pushing horizontally on the edge of top plate to create small horizontal oscillations, then count cycles (one back and forth movement). For example, 3 cycles in 6 seconds is 1/2 Hz. Depending on the damping, the isolator may only cycle 2 or 3 times.

VERTICAL NATURAL FREQUENCY

11. Check the vertical frequency by pushing down vertically on top plate to create small vertical oscillations, then count cycles (one up and down movement). 1/2 Hz is equal to one cycle in 2 seconds.

The vertical natural frequency can be changed using the vertical stiffness adjustment screw (G), although this adjustment is seldom necessary. This adjustment requires a 5/16 hex key. Turning the screw clockwise reduces the natural frequency, counterclockwise increases the frequency. This is a sensitive adjustment. Turn only a few degrees each time then check the vertical position and frequency. Adjust further, if necessary.

Note: Run any cables to the instrument with plenty of slack. Do not tie cables together as this will make them stiffer. Stiff and taut cables can stop the isolator from providing vibration isolation.

Bibliography

[1] K. Billon, N. Montcoudiol, A. Aubry, R. Pascual, F. Mosca, F. Jean, C. Pezerat, C. Bricault, and S. Chesné. Vibration isolation and damping using a piezoelectric flextensional suspension with a negative capacitance shunt. *Mechanical Systems and Signal Processing*, 140, 6 2020. ISSN 10961216. doi: 10.1016/j.ymssp.2020.106696.

[2] Linda Chen. Development of CRONE reset control. 2017. URL `https://repository.tudelft.nl/islandora/object/uuid:5370c610-4112-49e9-b860-9d625d5b40c5?collection=education`.

[3] R. B. Davis and M. D. McDowell. Combined Euler column vibration isolation and energy harvesting. *Smart Materials and Structures*, 26(5), 4 2017. ISSN 1361665X. doi: 10.1088/1361-665X/aa6721.

[4] Arnfinn A. Eielsen, Marialena Vagia, J. Tommy Gravdahl, and Kristin Y. Pettersen. Damping and tracking control schemes for nanopositioning. *IEEE/ASME Transactions on Mechatronics*, 19(2):432–444, 2014. ISSN 10834435. doi: 10.1109/TMECH.2013.2242482.

[5] Arnfinn Aas Eielsen and Andrew J. Fleming. Passive shunt damping of a piezoelectric stack nanopositioner. In *Proceedings of the 2010 American Control Conference, ACC 2010*, pages 4963–4968. IEEE Computer Society, 2010. ISBN 9781424474264. doi: 10.1109/acc.2010.5530938.

[6] A J Fleming and S O R Moheimani. Adaptive piezoelectric shunt damping. Technical report, 2003.

[7] A J Fleming, S Behrens, and S O R Moheimani. Reducing the inductance requirements of piezoelectric shunt damping systems. Technical report, 2003.

[8] Andrew J. Fleming and S. O. Reza Moheimani. Control Orientated Synthesis of High-Performance Piezoelectric Shunt Impedances for Structural Vibration Control. *IEEE Transactions on Control Systems Technology*, 13(1):98–112, 2005. ISSN 15580865. doi: 10.1109/TCST.2004.838547.

[9] Colin G. Gordon. Generic vibration criteria for vibration-sensitive equipment. In *Optomechanical Engineering and Vibration Control*, volume 3786, pages 22–33. SPIE, 9 1999. doi: 10.1117/12.363802.

[10] J. A.B. Gripp and D. A. Rade. Vibration and noise control using shunted piezoelectric transducers: A review, 11 2018. ISSN 10961216.

[11] J. A.B. Gripp, L. C.S. Góes, O. Heuss, and F. Scinocca. An adaptive piezoelectric vibration absorber enhanced by a negative capacitance applied to a shell structure. *Smart Materials and Structures*, 24(12), 11 2015. ISSN 1361665X. doi: 10.1088/0964-1726/24/12/125017.

[12] N.W. Hagood and A. von Flotow. Damping of structural vibrations with piezoelectric materials and passive electrical networks. *Journal of Sound and Vibration*, 146(2):243–268, 4 1991. ISSN 0022460X. doi: 10.1016/0022-460X(91)90762-9. URL `https://linkinghub.elsevier.com/retrieve/pii/0022460X91907629`.

[13] Xu Han, Marcus Neubauer, and Jörg Wallaschek. Improved piezoelectric switch shunt damping technique using negative capacitance. *Journal of Sound and Vibration*, 332(1):7–16, 1 2013. ISSN 10958568. doi: 10.1016/j.jsv.2012.08.001.

[14] Oliver Heuss, Rogério Salloum, Dirk Mayer, and Tobias Melz. Tuning of a vibration absorber with shunted piezoelectric transducers. *Archive of Applied Mechanics*, 86(10):1715–1732, 10 2016. ISSN 14320681. doi: 10.1007/s00419-014-0972-5.

[15] B J Joziasse. Department of Precision and Microsystems Engineering Nanometer precision scanning dual stage with reduced Joule heating in the fine stage actuator. (March), 2017.

[16] Melvin Kruik. Location optimized hybrid damping for one-dimensional flexible structures. 2020.

[17] R. Le Breton, G. Deleglise, J. Allibe, A. Badel, G. Balik, B. Caron, A. Jeremie, J. Lottin, and S. Vilalte. Nanometer scale active ground motion isolator. *Sensors and Actuators, A: Physical*, 204:97–106, 2013. ISSN 09244247. doi: 10.1016/j.sna.2013.09.020.

[18] Donald J. Leo. *Engineering Analysis of Smart Material Systems*. John Wiley and Sons, 1 2008. ISBN 9780471684770. doi: 10.1002/9780470209721.

[19] Yabin Liao and Henry A. Sodano. Piezoelectric damping of resistively shunted beams and optimal parameters for maximum damping. *Journal of Vibration and Acoustics, Transactions of the ASME*, 132(4): 0410141–0410147, 8 2010. ISSN 10489002. doi: 10.1115/1.4001505.

[20] Boris Lossouarn, Olivier Thierry, Mathieu Aucejo, and Jean-François Deü. Comparison of passive inductor designs for piezoelectric shunt damping. In *Active and Passive Smart Structures and Integrated Systems 2016*, volume 9799, page 97991S. SPIE, 4 2016. ISBN 9781510600409. doi: 10.1117/12.2219200.

[21] Youhei Miyaoka, ; Minoru, and Kuribayashi Kurosawa. Measurement of Current Noise and Distortion in Resistors. Technical report.

[22] S O Reza Moheimani, Andrew J Fleming, Springer Berlin, Heidelberg Newyork, Hong Kong, London Milan, and Paris Tokyo. Piezoelectric Transducers for Vibration Control and Damping. Technical report, 2006.

[23] Marcus Neubauer, Robert Oleskiewicz, Karl Popp, and Tomasz Krzyzynski. Optimization of damping and absorbing performance of shunted piezo elements utilizing negative capacitance. *Journal of Sound and Vibration*, 298(1-2):84–107, 11 2006. ISSN 10958568. doi: 10.1016/j.jsv.2006.04.043.

[24] Dominik Niederberger, Manfred Morari, and Stanislaw J. Pietrzko. Adaptive resonant shunted piezoelectric devices for vibration suppression. In *Smart Structures and Materials 2003: Smart Structures and Integrated Systems*, volume 5056, page 213. SPIE, 8 2003. doi: 10.1117/12.483388.

[25] David L. Platus. Negative-stiffness-mechanism vibration isolation system. In *Vibration Control in Microelectronics, Optics, and Metrology*, volume 1619, pages 44–54. SPIE, 2 1992. ISBN 0819407577. doi: 10.1117/12.56823.

[26] Robert Munnig Schmidt, Georg Schitter, and Jan van Eijk. *The Design of High Performance Mechatronics*. Delft University Press, 2011. ISBN 9781607508250. doi: 10.3233/978-1-60750-826-7-i.

[27] Jan Van Eijk. on the Design of Plate-Spring Mechanisms. *Technische Hogeschool Delft, Afdeling der Werktuigbouwkunde (Report) WTHD*, (172), 1985.

[28] Keisuke Yamada, Hiroshi Matsuhisa, Hideo Utsuno, and Katsutoshi Sawada. Optimum tuning of series and parallel LR circuits for passive vibration suppression using piezoelectric elements. *Journal of Sound and Vibration*, 329(24):5036–5057, 11 2010. ISSN 0022460X. doi: 10.1016/j.jsv.2010.06.021.

[29] U. Zabit, O. D. Bernal, and T. Bosch. A self-mixing displacement sensor compensating parasitic vibration with a MEMs accelerometer. *Proceedings of IEEE Sensors*, 36(5):1386–1389, 2011. doi: 10.1109/ICSENS.2011.6126997.